Chapter 4

Data Analysis Tools

4.1 Tracker

At least three different track-finding programs were written and used by the MiniMax collaboration [49]. Each has a different algorithm for reconstructing tracks from hit wires, but all give similar results.

The work described here was done using the combinatorial tracker. That algorithm is constructed to find all possible combinations of the hit wires in four "crosshair chambers". At least three of these chambers have different orientations, so that a unique straight line can be drawn through any such combination of hits. The line is considered a potential track, and the non-crosshair chambers are searched for hit wires within 3.5 wire spacings of the line. If enough wire hits are found, a straight line is fit to the hits. Then, if the fitted track passes quality cuts such as cuts on the χ^2 of the fit, the track is recorded. Several sets of crosshair chambers are used in order to increase the probability that a track and all the associated hit wires are found.

Tracks with a greater number of wires are always looked for first because they are more likely to be the correct track than a similar one with fewer wires; when two tracks are similar (have a large fraction of wires in common) the track found first has more weight in determining the track parameters. Also, the tracker code is written to search for tracks which are pointed such that they appear to originate near the collision point before allowing the tracks to point in any direction. Tracks are searched for in the following order. First the charged tracks that go straight through the detector are found and recorded. Then the tracking is run on the back 16 chambers and tracks which do not share too many wires (the exact numbers are given in Table 4.1) with previously-found charged tracks are recorded. These tracks include photon conversion tracks and segments of charged tracks which bend in the lead and are therefore not found as through-going charged. Tracks of the same type are then looked for in the eight chambers directly behind the lead (chambers 9-16) in case the tracks leave the acceptance before hitting enough chambers. Interactions in the beam pipe also produce background tracks which can be found in this region. Finally, the front eight chambers are searched for segments of charged tracks that are not found as going straight through all chambers. Figures 4.1-4.6 show event displays of various types of tracks.

In the process of searching for each type of track, track candidates are compared to previously-found tracks to make sure that the same real track is not being recorded as many similar tracks. In the charged tracking, for example, tracks with hit wires in at least 22 chambers are searched for first. After a track is found, the wires hit by the track are stored in a list of used wires. As each new track candidate is found, its wires are checked against the used wires. If the candidate does not have at least 17 unique wires hit, it is dropped. This significantly reduces the number of fake tracks recorded by the tracker. The candidate track is also compared to the other tracks individually. The hits in each chamber are compared, and if the tracks are within two wires of each other in at least 16 chambers, the tracker determines that the same track has been found and the hits of the current candidate are added to the list of hits in the previously-found track. We refer to this as "grouping". Wires from the grouped track are added to the used-wire list. Next, tracks which go through only 21 chambers are considered. If such a track candidate has more than 17 wires which are in the used-wire list, the candidate is dropped, and if it has 16 wires within two wire spacings of hits in another track, the two tracks are grouped. Table 4.1 shows the various cuts on number of chambers hit or wires in common for each type of track.

The tracks are broken into segments in front of and behind the converter plane, referred to as "heads" and "tails", respectively. A dst is written, which, though traditionally stands for data summary tape, is just a file which contains, for each event, the event number, number of heads and number of tails, and then for each track segment, the number of wires hit followed by the list of wires. The wire number is given by $(\text{chamber} - 1) \times 128 + \text{wire}$, for chambers 1-24 and wires 1-128 in each chamber. Earlier dst formats included the NHITS of the event (which can still be retrieved from the run data file) and the track parameters determined by a fit (which are now determined using separate code, as discussed in the next section). Sample dst entries are shown in Figs. 4.7, 4.8. The tracker is run once for each actual or simulated run, and the dst is used in all further analysis.

Only events with an NHITS less than 600 have been analyzed by the tracker. Higher-NHITS events tend to have large hit densities in the rear chambers, which leads to a huge number of potential tails, most of which are not real charged or photon-conversion tracks, and the tracker takes a longer time to analyze these events. About 6% of the events in lead-in runs have NHITS higher than this value. The NHITS is correlated with multiplicity, so that the sample of events which were analyzed by the tracker is somewhat biased towards lower-multiplicity events.

4.2 Track fitter

A separate program is necessary to fit tracks from the wires written in a dst since the fit parameters from the combinatorial tracker are calculated in the (x, y) coordinate system instead of in (u, v) (this is important because the resolution in u is much better than in v in the chambers behind the lead) and uncertainties in the track parameters are not reported. The code for the track fitter is given in Appendix B. With the track fitter, straight lines are fit to the hit wires in a track, parameterized by $u(z) = a_u + b_u z$ and $v(z) = a_v + b_v z$, and the covariance matrix (which gives the correlated uncertainties of parameters [50]) is generated. Uncertainties in the position of the track at a chamber are taken to be $1/\sqrt{12}$ [1] times the wire spacing for all hits.

Another subroutine (see Appendix B) is used to correct a small problem with tracks found by the tracker. Occasionally (in about 10% of the events), a tail is recorded which, in a single chamber, includes two wires as part of the same track which are separated by several wires; these double hits are present in most of the non-u chambers of the track.

The cause turned out to be that two track candidates have common wires in all of the u-chambers, and enough close wires in other chambers for the tracker to group the track candidates into one track. In some cases, the candidates which are grouped in this way are two real tracks, but more often one of the candidates is a type of fake track which will be referred to as a "ghost". (A ghost is a track which borrows hits in the u chambers from a single real track, and finishes up the track with random hits in the non-u

[1]For a hit to be recorded in a single wire in a chamber, a charged track must pass within 1 wire spacing of that wire. The uncertainty in position is then given by $(\Delta x)^2 = \langle x^2 \rangle - \langle x \rangle^2 = \int_0^1 dx\, x^2 - (\int_0^1 dx\, x)^2 = 1/12$, where x is the distance in units of wire spacings.

chambers such as from pipe-shower secondaries.) The track which is recorded is halfway between the two candidates.

Since the occurrence of these tracks with double hits is fairly rare, especially for those made of two real tracks, we do not try to separate out two distinct tracks, but rather to find one good track. The code used to correct this problem tries all possible combinations of hit wires such that the non-u chambers each have only one wire included in the track. Only two of these combinations are considered as potential correct tracks: the one which best points (in v) towards the collision point, and the one which has the best χ^2 when fit to a line in the v-z plane. Of course, a single combination can satisfy both these requirements.

The pointing in v is somewhat complicated by the fact that tracks going through the acceptance are at very small angles from the $v = 0$ plane. Therefore, the uncertainty of the z for which $v = 0$ is much larger than that of $z(u = 0)$. In other words, the uncertainty in the angle between the track and the $v = 0$ plane and that angle are both comparably small. Instead, we use the following measure of pointing in v. We find the z for which $u = 0$ for the track, defined as z_0. Then, working in the v-z plane, we define θ_0 as the angle between the z-axis and a line drawn from $(v = 0, z = z_0)$ to the point where the track being considered intersects the lead. The angle between the track itself and the z-axis in the v-z plane is defined as θ, and the uncertainty in that angle as σ_θ. The measure of pointing is taken to be

$|\theta_0 - \theta| / \sigma_\theta$, which is small for tracks which point (to within uncertainty) to the same z as is pointed to in u.

Figure 4.9 shows histograms of χ^2 for tracks with the best χ^2, $|\theta_0 - \theta| / \sigma_\theta$ for tracks with the best pointing, and then these values for good tails (those which did not have the double-hit problem). The plot of χ^2 for good tails has an obvious separation of what we believe are real tracks and background, which we use to choose the cut $\chi^2 < 7$. For the pointing in v, we require $|\theta_0 - \theta| / \sigma_\theta < 8$. We are most interested in tails which point back to the collision point. (Further discussion of pointing cuts is given in Sec. 4.3.) Therefore, if the track with the best pointing also passes the χ^2 cut, it is kept as a good track. If this is not the case, the track with the best χ^2 is considered, and kept if it passes the pointing cut. In most cases, none of the combinations of wires produce a track which passes the pointing cuts, and the track is dropped.

4.3 Vertexer

Charged tracks from the collision point and photon conversion tracks are then reconstructed from the track segments. The vertexer code, given in Appendix C, is used to determine the probability that track segments meet at a common point at the plane of the lead. A charged track is then defined as a head which either "matches" at least one tail or passes cuts discussed below, and a photon as any group of tails (or a single tail) not matched to anything in front of the lead. In terms of the notation (number of heads in match, number of tails in match), a charged track is a $(>0, \geq 0)$ and a photon is a $(0, >0)$. The location of the vertex is taken as the mean position of the included track segments at the lead, weighted by the uncertainties. In order to avoid effects from the edge of the lead, the vertex position is required to be within the region defined by $4.25\,\text{in} < u < 10.25\,\text{in}$, $-3\,\text{in} < v < 3\,\text{in}$, and $\sqrt{(u - 7.25\,\text{in})^2 + v^2} < 4\,\text{in}$, which is roughly the area 1 in from all sides of the lead.

The uncertainty in the position of the tail at the lead is apparently underestimated by propagating the uncertainties in track parameters calculated by the fitter. The most likely cause of this is multiple scattering in the lead. The mean variance in the u position from this error propagation is ${\sigma_u}^2 = 5.5 \times 10^{-4}\,\text{in}^2$ and in v is ${\sigma_v}^2 = 0.030\,\text{in}^2$. A new estimate was found by histogramming the distance between two conversion tracks from a single photon in GEANT at the lead, and taking the standard deviation of the histogram as the uncertainty in position. Figure 4.10 shows these histograms, which give the new values ${\sigma_u}^2 = 0.007\,\text{in}^2$ and ${\sigma_v}^2 = 0.092\,\text{in}^2$. (The order of magnitude is really more important than the specific value, since cuts on other variables used in the vertexer can compensate for small differences in these values.) Calculated uncertainties for a track segment which are less than the new values are increased to the new values in the vertexer.

Tracks are required to point to within some distance of the mean collision point in order to remove background such as tracks from beampipe shower, and also combinatorial fakes. Figures 4.11 and 4.12 show the z for which $u = 0$ of heads and tails of (1,1) charged tracks, and for single (0,1) photon conversion tails. Heads of charged tracks are required to point to the region $-50 < z < 60$, which includes almost all primary charged tracks. Most of the tracks outside this region are fakes, although some are decay products of neutral particles such as the K_s^0. Tails of charged tracks are not required to point so that tracks which multiple scatter in the lead will not be dropped. For lead-out runs (Fig. 4.11), most (0,1)'s which point to $z \gtrsim 50$ are tracks from interactions in the beampipe, while for lead-in runs (Fig. 4.12), many are from photon conversions in the lead. In order to cut out the fakes from pipe shower, single photon conversion tracks are required to point to $-40 < z < 50$. For photon conversions which produce more than one track, at least one track in the vertex must point to $z < 50$. The pointing cut in v is taken from the study in the previous section to be $|(\theta_0 - \theta)/\sigma_\theta| < 8$.

Parameters used in the vertexer code were determined by finding those which best reconstruct the PYTHIA and GEANT tracks, which are recorded in separate files. The pointing cuts, the increased uncertainties in the u and v position of tails, and cuts on the χ^2 for the fit of how well two tracks match at the lead (which will be discussed in Sec. 4.3.1, see Fig. 4.13) are not independent; the cuts chosen are all self consistent. The code seems to work sufficiently well for both simulated and real data. As an example, Fig. 4.14

shows the tracks which survived the vertexer cuts for the large NHITS event of Fig. 4.6.

Plots of efficiencies for finding charged tracks and photons are shown in Figs. 4.15-4.24. Efficiencies are given as a function of energy, transverse momentum, multiplicity, NHITS, and position in η and ϕ. The numbers of charged tracks and of photons in the acceptance as a function of these parameters are also shown, both because these distributions are interesting, and also to give an indication of the statistical significance of bins in the efficiency plots. The plots also include the mean number of fakes as a function of multiplicity and NHITS, and the mean number of actual charged tracks and photons as a function of NHITS.

4.3.1 Matching tracks at the lead

Tracks are "matched" or "vertexed" in the following way. Consider two tracks intersecting the lead at points $\boldsymbol{\xi_1} = ({\xi_1}^1, {\xi_1}^2) = (u_1, v_1)$, $\boldsymbol{\xi_2} = ({\xi_2}^1, {\xi_2}^2) = (u_2, v_2)$, with covariance matrices $\mathbf{C_1}$ and $\mathbf{C_2}$. Assume that the two tracks meet at exactly the same point $[\bar{\boldsymbol{\xi}} = (\bar{\xi}^{\,1}, \bar{\xi}^{\,2})]$ at the lead. Also assume that the $\boldsymbol{\xi}_i$ are Gaussian distributed about mean $\bar{\boldsymbol{\xi}}$.

The χ^2 for the fit of the two tracks to $\bar{\boldsymbol{\xi}}$ is

$$\chi^2 = (\boldsymbol{\xi_1} - \bar{\boldsymbol{\xi}})\mathbf{C_1}^{-1}(\boldsymbol{\xi_1} - \bar{\boldsymbol{\xi}}) + (\boldsymbol{\xi_2} - \bar{\boldsymbol{\xi}})\mathbf{C_2}^{-1}(\boldsymbol{\xi_2} - \bar{\boldsymbol{\xi}}). \tag{4.1}$$

Minimizing χ^2 with respect to $\bar{\xi}^{\,i}$ gives

$$\bar{\xi}^{\,i} = \left[(\mathbf{C}_1{}^{-1} + \mathbf{C}_2{}^{-1})^{-1}\right]^{ij} \left[(\mathbf{C}_1{}^{-1})^{jk}\xi_1{}^k + (\mathbf{C}_2{}^{-1})^{jk}\xi_2{}^k\right]. \qquad (4.2)$$

Putting this $\bar{\boldsymbol{\xi}}$ back into Eq. 4.1 yields χ^2. There are four known parameters ($\boldsymbol{\xi_1}$ and $\boldsymbol{\xi_2}$), and two which are determined ($\bar{\boldsymbol{\xi}}$), leaving two degrees of freedom. The reduced χ^2 is therefore $\chi^2/2$.

All track segments in an event were matched together in order to find the cutoff in $\chi^2/2$ for which matches with a lower χ^2 are most likely real tracks, while those with a higher χ^2 are most likely unrelated track segments. Plots of matches between pairs of heads, pairs of tails, and head-tail pairs are shown in Fig. 4.13. Head-head matches which have a low χ^2 are due only to the heads being coincidentally close together at the lead. The peak at low $\chi^2/2$ for head-tail matches is due to charged tracks, and is fairly cleanly separated from false matches. The tail-tail plot does not show a clear division, but a slight division is present at about the same value of $\chi^2/2$ as the division for head-tail matches. (Note that the cutoff values could have been different for the head-tail and tail-tail matches since the uncertainties in position of the tails are much larger than those for heads.) A reasonable cut appears to be $\log(\chi^2/2) < 0.7$, or $\chi^2/2 < 5$.

4.3.2 Tracks which may be grouped together

The original vertexer algorithm grouped any track segments which matched any other track segments in a vertex. The uncertainty in position of the tails is large enough that this occasionally produced vertices which contained more than one real track. For instance, a (1,1) charged track and a (0,n) photon could be grouped into a (1,n+1), or two charged tracks could become a (2,2).

By demanding that all tails in a vertex match the head (which has a much smaller uncertainty), charged tracks are less likely to be grouped with other tracks. The vertexer code was therefore changed to look for charged tracks first and remove those tails which were matched to heads before matching tails together. The following is the result of this change for a sample of GEANT events.

Of the original 135 (2,2) vertices, 104 have heads which do not match each other and were therefore separated. About 94% of these are really two charged tracks, and 6% are fake heads grouped with real tracks. The 31 vertices which have two heads that match each other consist of 48% fake heads along with other tracks, 13% e^+e^- pairs from photon conversions in the window ("window conversions"), and 39% vertices with two charged tracks which are very close together at the lead.

The majority of (1,n)'s which were separated into more than one vertex are charged tracks combined with tails from photons, fake tracks, or pipe shower tracks. The latter two types of tails are likely to be removed by pointing cuts when separated from the charged track. About 10% result from window conversions where a conversion secondary showers in the lead, and approximately 5-10% are single charged tracks with multiple tails (from interactions in the lead). Of those which remained (1,n)'s, approximately 20% are pions which interact in the lead, 30% are pairs of a charged track and a fake tail, 25% result from window conversions, and 20% are pairs of a close charged track and a photon. The rest involve missing heads, decays in GEANT, etc. Only about half of the vertices which contained both a charged track and a photon were reclassified as such.

The overall improvement in vertexer performance due to these changes is small since these types of vertices are not very common. Efficiencies are improved for high multiplicity events, without introducing many fakes.

Studies were also done with the real data by adding a single charged track or photon conversion track from a clean event to every other event in the run. This was done at the level of the dst, so that the behavior of the tracker for the combined events is ignored. At this level, the efficiencies for finding all tracks of the individual events in the combined event are not compromised unless the added track is within some distance of a track in the other event. The mean distance between an added charged track and another charged track for a track to be missed is about 0.5 in, and for an added charged track and a photon conversion about 0.7 in.

4.3.3 Tail-less heads as charged tracks

Often the tail of a low-energy charged track will not be detected due to multiple scattering in the lead which may cause it to stop or to bend out of the acceptance or to lose so much energy that it does not travel in a straight path through the rear chambers. In GEANT, most of the (1,0)'s are real (collision-point) charged tracks which stopped in the lead or had very soft tails; some are from neutral particle decays. Those tail-less heads which are fakes are distinguished by the fact that they do not have hits in all eight of the front chambers. However, in the real data, the (1,0)'s seem to include a large fraction of fakes. The ratio of the number of (1,0)'s to the total number of identified charged tracks [including (1,0)'s] is much higher for the real data (run 1125) than for GEANT, 17% vs 7%, whereas if the energy distributions of charged tracks are similar for real data and GEANT, this fraction should be about the same. Eliminating those (1,0)'s which do not have hits from all eight chambers reduces the fractions to 12% and 6%. Other types of (1,0)'s which appear to be fakes either share wires in all three u or all three v chambers with another track (ghosts), or point to somewhere other than the intersection with the z-axis (in u) of other charged tracks in the event which go all the way through the detector.

Based on these observations, tight cuts are made which are intended to eliminate most fakes at the expense of losing some real charged (1,0)'s. Any (1,0)'s which share wires in all u or all v chambers are dropped. The pointing cut is defined by other charged tracks in the event; if there are none, it is not used. The collision point z_{cp} is determined as the weighted mean of the point of intersection with the z-axis of any other heads of (1,> 0) charged tracks in the event, using the parameterization in u of the heads and the associated uncertainties. Plots of the distance between the $z(u = 0)$ of the (1,0) and the mean z_{cp} divided by σ, the root mean square of the uncertainty in these z, for both GEANT and real-data (1,0)'s are used to choose the condition that the $z(u = 0)$ of the (1,0) must be within 2σ of z_{cp}. This cuts out many real charged (1,0)'s. These cuts reduce the ratio of "charged" (1,0)'s to total charged tracks to 5.0% for GEANT and 9.6% for run 1125. Although the fraction for the data is almost twice as large as that for the GEANT, no apparent qualities of the remaining (1,0)'s suggest that they are fake.

4.3.4 Middle-eight tracks

Originally, tails which do not go through at least 14 of the rear chambers, but do go through the first eight chambers behind the lead were not used by the vertexer. The reason is that the rear chambers are often flooded with pipe shower, which results in a large number of "middle-eight" tracks which are pipe shower tracks or combinatorial fakes which can be found as photon tracks by the vertexer. However, these tracks can be used carefully in certain circumstances. Allowing the middle-eight tracks to be vertexed as tails of charged tracks saves some real charged tracks that would otherwise be (1,0)'s and might have be thrown away by the tight cuts. The vertexer also allows middle-eight tracks as photon conversions as long as they are vertexed with at least one other tail. This is important because the tight pointing cuts on (0,1) photons are often failed by a single tail of a photon conversion which produces other tracks that leave the acceptance before reaching the final chambers. If a middle-eight tail is vertexed to such a tail then the vertex is not subject to the tight cuts. Also, since fake tracks are unlikely to vertex at the lead, a vertex made only of at least two middle-eight tracks is counted as a photon.

It turns out that very few events have middle-eight tracks which can be vertexed with other track segments at the lead, so that the effect on overall efficiencies is almost negligible. This may be related to the difficulty of getting a good fit for middle-eight tracks due to the lack of v-resolution. Fake charged tracks are occasionally created when a fake (1,0) is coincidentally matched with a middle-eight tail. The middle-eight tracks were nevertheless included in the vertexing, since even a tiny improvement in the photon-finding efficiencies is welcome.

4.3.5 Origin of fakes

A charged track from the vertexer is classified as a fake if there are no charged tracks from PYTHIA inside the acceptance within the specified distances in u and v of 0.5 in and 1 in, respectively, of the identified track at the lead. A sample of events which have one fake charged track was taken from 1.5×10^5 GEANT events. In order to avoid effects due to the presence of photons, the events were required to have no photons observed or known to convert in the acceptance. The sample is divided into the following categories: events in which 0, 1, or 2 charged tracks are sent into the acceptance and one extra charged track is found (the total sample of events had 3402, 1475, 348 events, respectively, in these classes, and 39, 38, and 38 events were used in this study), and those in which 0 charged tracks are sent into the acceptance and 2 are found (217 total events, 37 events used, accounting for 74 fake tracks). Of the 188 fake charged tracks,

150 are decay product(s) of K_s's or Λ's,

24 are secondary charged tracks from other decays or interactions in the material surrounding the detector

1 is from the conversion of a photon in the window,

12 are real charged tracks just outside the acceptance, and

1 is an actual combinatorial fake.

Decays of single K_s's or Λ's are responsible for about 70% of the events with two fake charged tracks. The important outcome of this study is that almost all of these "fakes" are caused by interesting physics processes or edge effects.

Also studied were 20 events (from a total of 416) where a photon conversion is present in GEANT[2] and that photon is not found, and no PYTHIA

[2]GEANT conversions are defined as $e^\pm$ tracks originating in the region containing the lead and scintillator between chambers 8 and 9, and within 0.1 in at the lead of a photon

charged tracks are sent into the acceptance, but one is found. In 11 of these events, the photon converts in the window, and a resulting $e^{\pm}$ showers in the lead, i.e., the missed photon and fake charged track are correlated. The remaining events involve photons which are not found by the vertexer or are found just outside the acceptance, with uncorrelated fake charged tracks which fall into the categories mentioned above.

A photon found by the vertexer is defined as fake if no PYTHIA photon is aimed such that it will hit the lead within 0.5 in in u and 1 in in v of the identified conversion. In 38 events (from a total of 1800) where no charged tracks are sent into the acceptance by PYTHIA and no photon conversions from GEANT are present in the acceptance, and one photon is found,

19 are conversions of secondary photons, roughly half of which appear to be due to decays, and the other half due to interactions in the detector region,

14 are real photons just outside the acceptance,

2 are charged decay products of K_s's where the heads are lost,

1 is the product of an interaction of a neutron in the lead, and

2 are from events which are too complicated to determine the source of the fake.

Of 20 events (from a total of 319) where a charged particle is lost and a fake photon found, 17 involve a charged track which multiple scatters in the

---

from PYTHIA.

lead so that the tail is found as a photon conversion, but the head is dropped. In the remaining 3 events, the missed and fake tracks are uncorrelated.

When a pipe shower produces a large density of hits in the rear chambers, the probability is greatly increased for finding fake photons. Combinations of these hits, possibly together with hits from real tracks from the collision, form tracks which point to the collision region and therefore should be found by the tracker. Ghosts (described in Sec. 4.2) are a common example of such a fake track.

If pipe showers were uncorrelated with important observables such as the number of charged tracks and photons entering the acceptance in an event, then vetoing events which have pipe shower would reduce the number of fake photons found without biasing the remaining sample of events, say towards those with low multiplicity. Unfortunately, this is not the case. In order to study this, we first identified events with pipe-shower tracks. Primary tracks which are produced in the collision and pass all the way through the MWPC telescope occupy a very limited region of the phase space defined by the position and angle in u at some z. (Recall that the acceptance is roughly defined by the coverage of the lead converter, which extends from $u = 3.25$ in to 11.25 in and $v = -4.0$ in to 4.0 in at $z_{lead} = 150$ in.) Figure 4.25 shows the location of tracks in (u, θ_u) space where $u = u(z_{lead})$ and $tan\theta_u = u(z_{lead})/z_{lead}$, averaged over many events. The dense band near the center of the plot is due to primary charged tracks. We defined rough boundaries around this region and vetoed events with any tails in the regions $\theta_u > 0.009u + 0.016$ or $\theta_u < 0.006u - 0.028$, excluding tails which the vertexer found as photon conversion tracks. (Note that this is a very tight cut.)

Because of the higher hit density in the rear chambers created by pipe shower, the events which remain after the pipe-shower veto have a much lower mean NHITS than that for all events. In GEANT, the mean NHITS for lead-in runs dropped from 142 to 90, and in run 1125 (lead in) from 229 to 113. Also, surviving events with higher NHITS tend to have more real tracks, as is shown for GEANT in Fig. 4.26. This figure also shows the distributions of actual charged-track and photon multiplicities (from PYTHIA), which appear to be biased towards lower multiplicities. This seems to be true to a greater extent for the real data; Figure 4.27 shows that the probability distribution of the observed number of photons before and after the pipe-shower veto for real data is more biased towards lower multiplicities than that for GEANT. The mean number of charged tracks found decreased from $\langle n_{ch} \rangle = 0.53$ for all GEANT events to 0.47 for this sample, and of photons from $\langle n_\gamma \rangle = 0.21$ to 0.14. For the data (run 1125), the cut is even harder: $\langle n_{ch} \rangle = 0.48$ falls to 0.32 and $\langle n_\gamma \rangle = 0.19$ drops to 0.06, practically no photons. We expect the veto to have a greater effect on the data because we believe that the real events contain more pipe shower than the GEANT, but since the vetoed events are apparently correlated with high multiplicity events, the remaining events are a clean, but not unbiased, sample.

This sample of non-pipe-shower events is useful for studying fake photons which were not caused by pipe shower, although the events are also less likely to contain converted photons. Fake photons in two sets of the remaining events were classified. The first set was taken from about 10^4 minimum-bias (triggered) events, and contains 104 events which pass the pipe-shower veto and have a fake photon. The second contains 71 such events which also have at least four primary charged particles and/or photons (from PYTHIA) in the acceptance; this sample includes all events of that type in the approximately 1.5×10^5 triggered events.

Of the fakes in the first set,

5 are ghosts,

11 are tails of charged tracks which are not vertexed with the heads,

9 are associated with photon conversions but are not vertexed with the other conversion tracks,

31 are other secondary photons such as those produced by interactions in the beampipe,

2 are secondaries from the interactions of neutrons in the lead,

11 are photons from the decays of π^0's produced by $K_s \rightarrow \pi^0\pi^0$,

18 are real photons just outside the acceptance,

and the remaining 17 either are not able to be classified, or fell into unique categories. The first few types of fakes are the most serious because they are correlated with the presence of real tracks. In almost all cases, when the tail of a charged track is not vertexed to the head, the tail-less head does not pass the cuts necessary to be counted as a charged track. Therefore a charged track is lost and is replaced by a fake photon. (This complicates the generating function analysis described in Chapter 5, because it introduces a correlation between charged-track and photon efficiencies.) The classification of photons which are outside the acceptance but are found inside the acceptance as fakes is really just due to details in the code for finding fakes.

Due to the higher multiplicities in the second set, we expect more fakes associated with real tracks, such as ghosts. We find that this is true, but not to an extent which would seriously invalidate the assumptions made in the next chapter. The fake photons include

8 ghosts,

25 tails of charged tracks,

12 tracks associated with a photon conversion,

11 other secondary photons,

2 photons from $K_s \rightarrow \pi^0\pi^0$,

9 photons just outside the acceptance,

and 4 unclassified fakes.

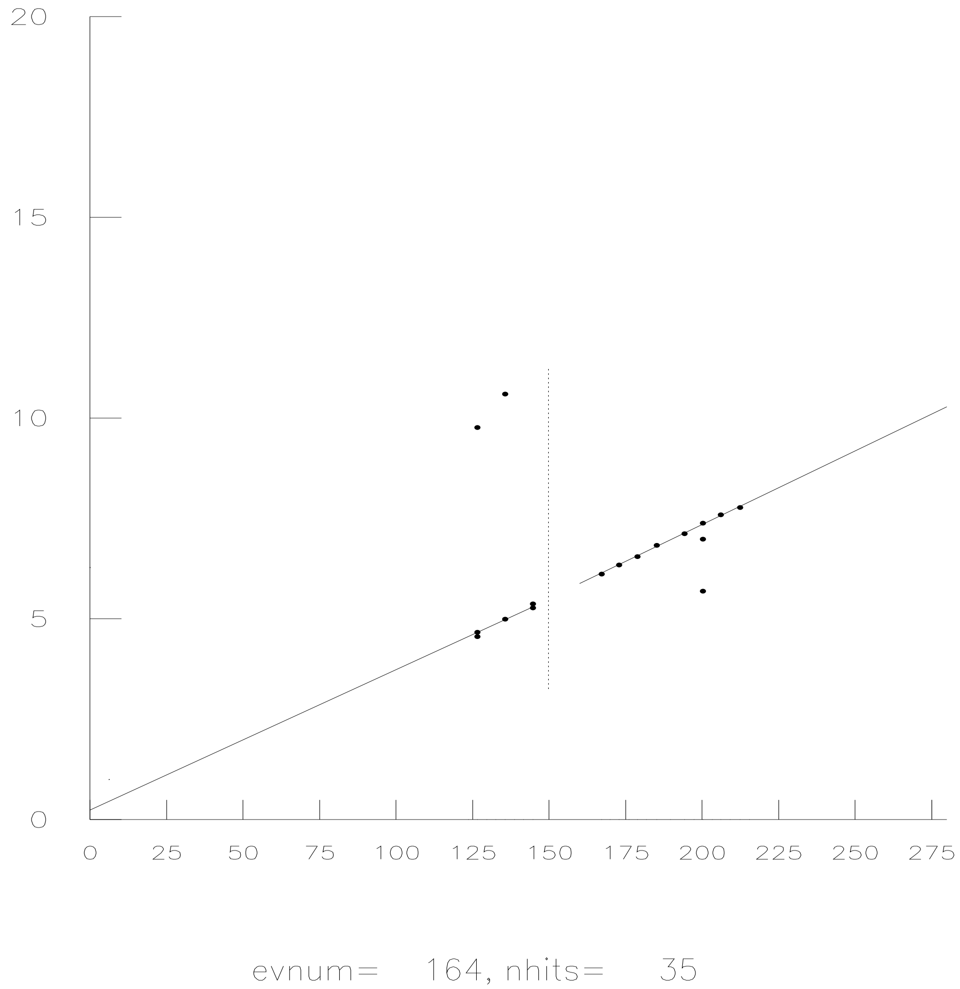

Figure 4.1: Event display of a clean charged track.

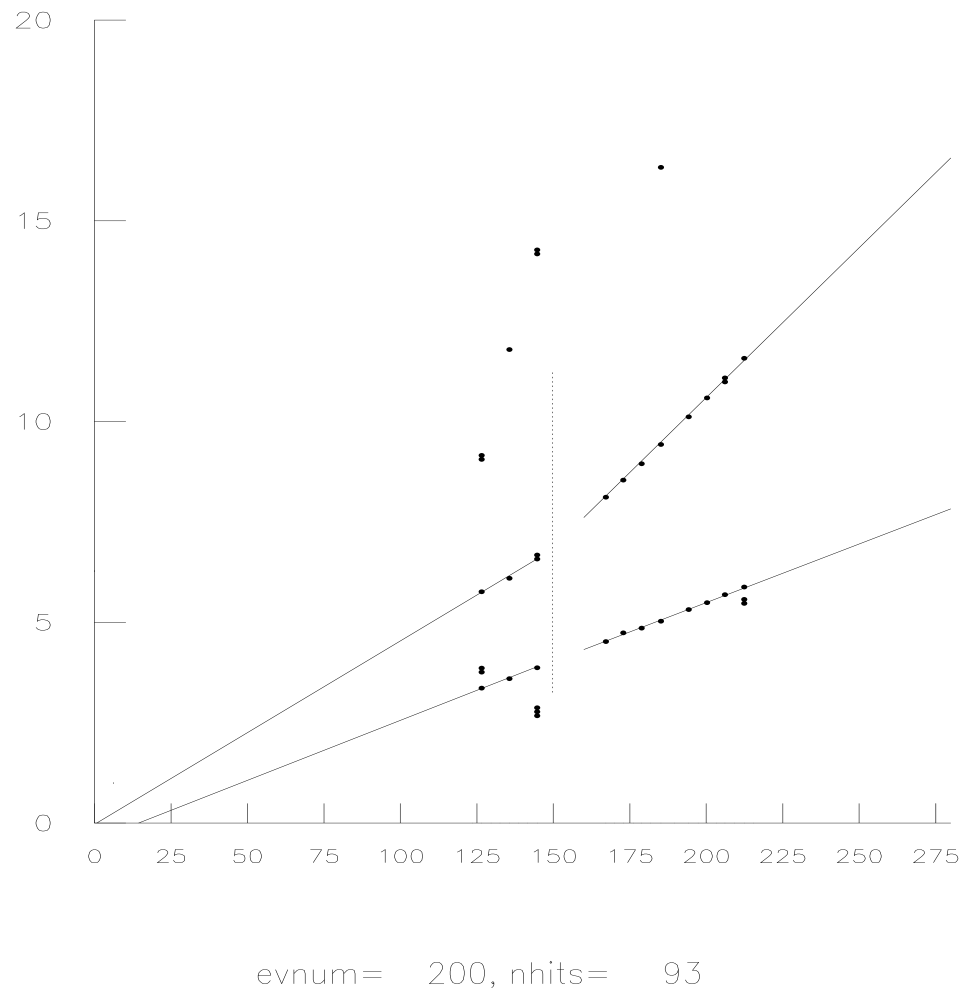

Figure 4.2: Event display of a straight-through charged track and a charged track which bends in the lead.

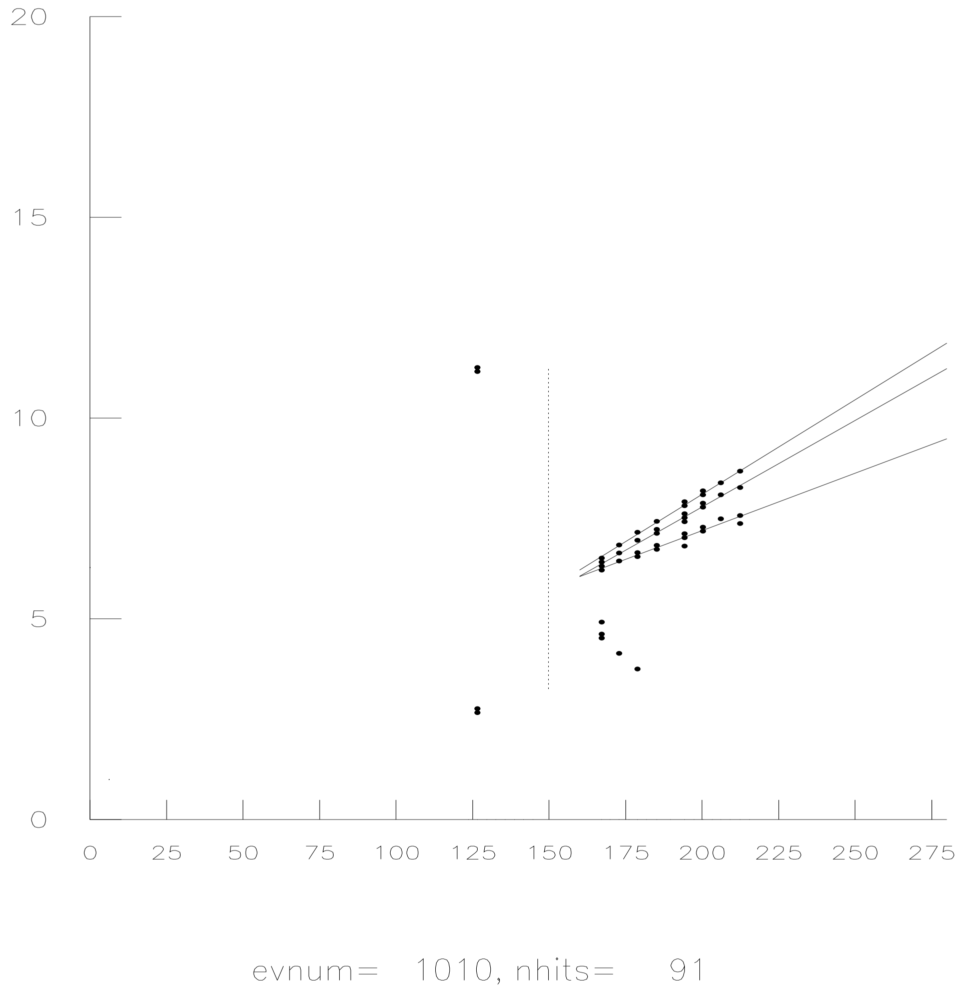

Figure 4.3: Event display of a photon with three conversion tracks.

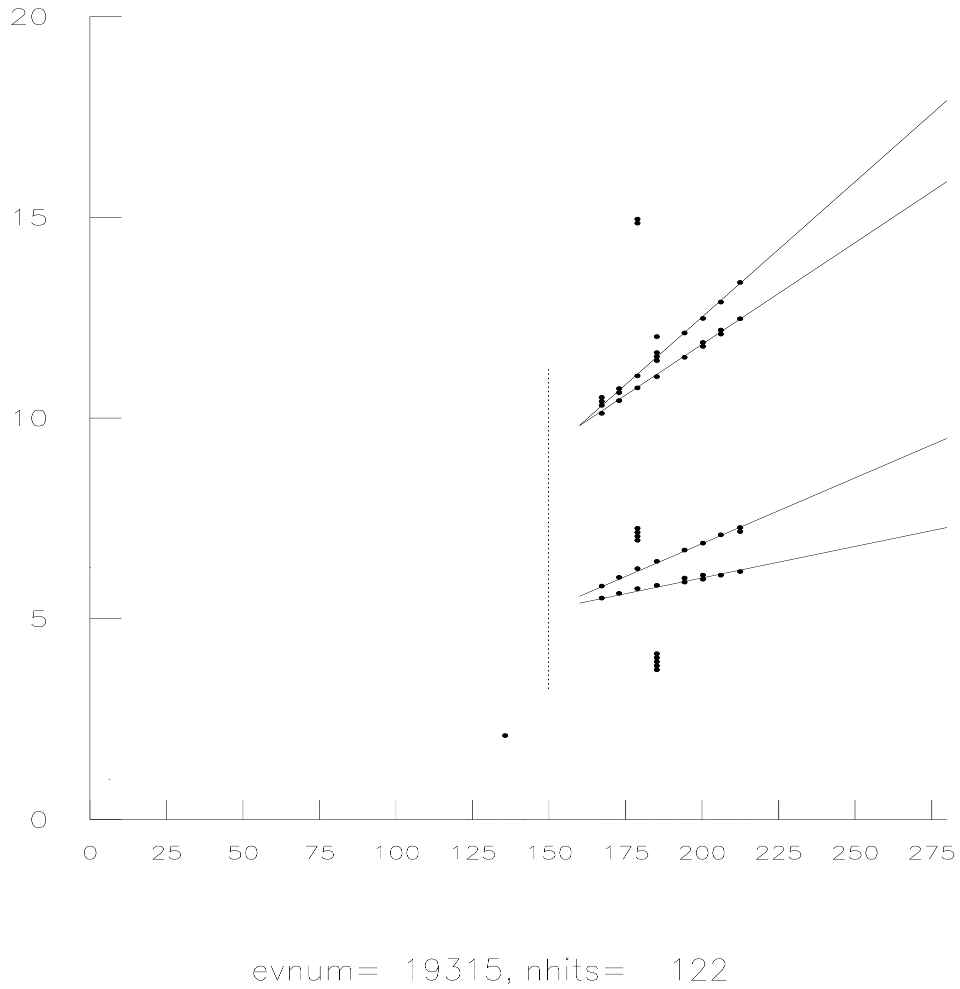

Figure 4.4: Event display of two clean photon conversions.

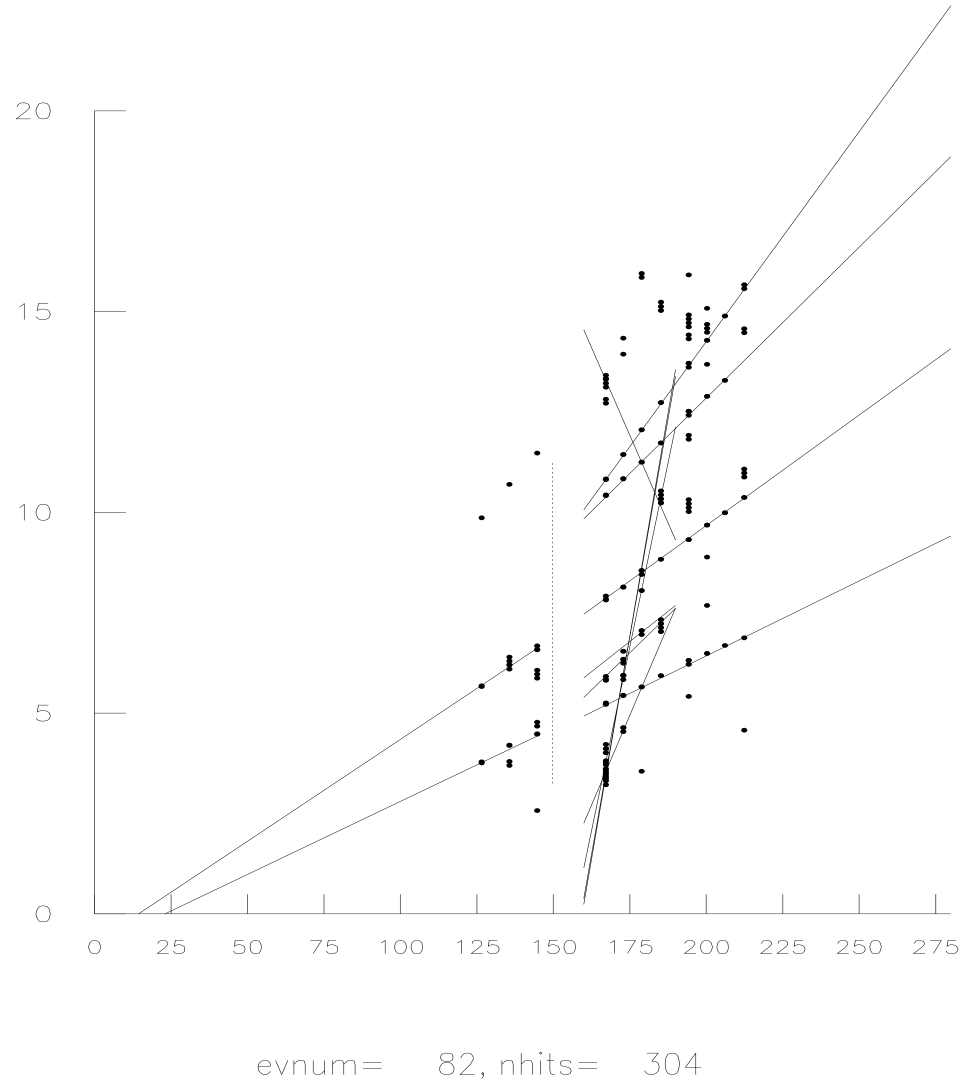

Figure 4.5: Display of an event with two charged tracks and a photon, and typical NHITS.

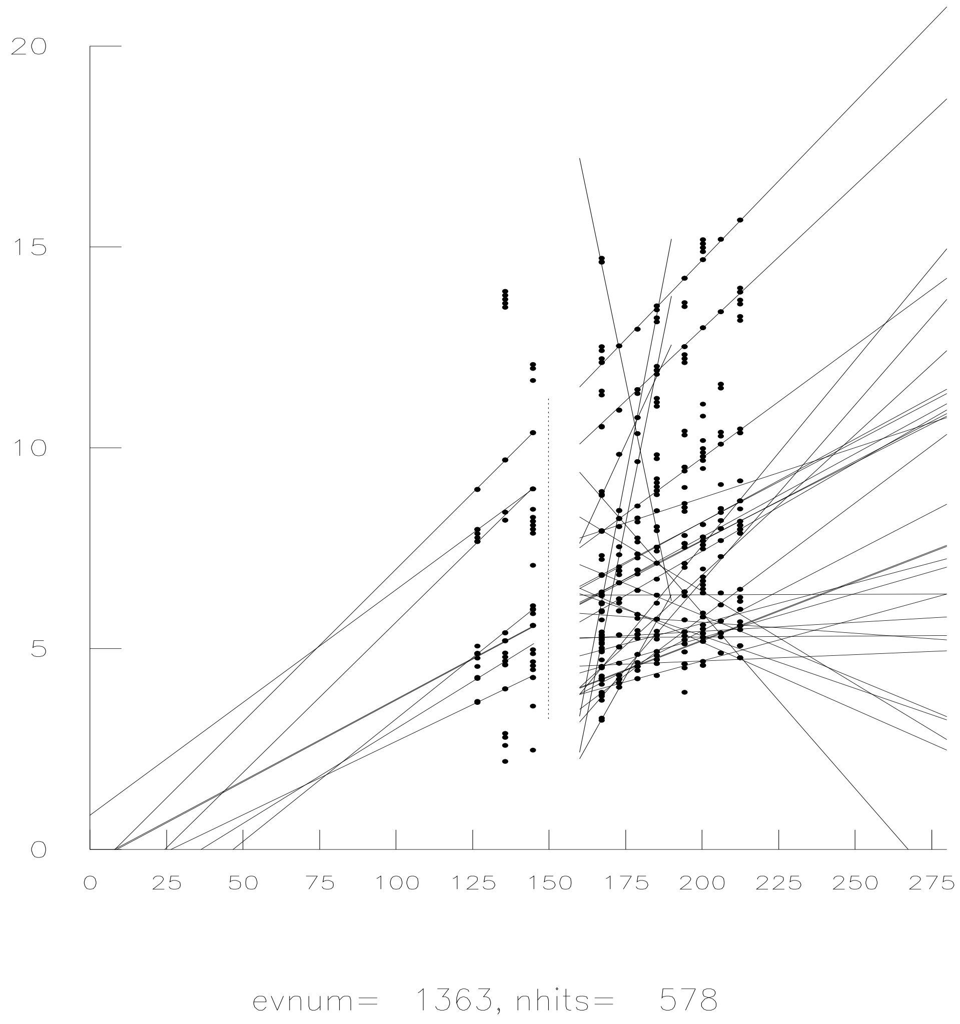

Figure 4.6: Display of an event with a large NHITS.

```
   164        1        1
          7
  77   328   485   610   694   870   927
         15
1055  1249  1377  1440  1633  1761  1888  1955  2144  2273  2337  2655
2730  2850  2979
```

```
  1010        0        3
         15
1058  1241  1374  1436  1629  1763  1884  1965  2140  2264  2341  2650
2745  2855  2977
         19
1057  1056  1241  1242  1376  1433  1632  1766  1888  1960  2144  2269
2335  2533  2656  2737  2846  2848  2969
         15
1059  1239  1372  1439  1627  1758  1882  1965  2136  2264  2344  2647
2741  2859  2986
```

Figure 4.7: Entries in the dst for the events shown in Figs. 4.1 and 4.3.

```
    82         2        11
          8
  52   240   298   501   618   659   870   919
          8
  82   221   336   472   598   705   860   940
         14
1046  1248  1386  1421  1642  1778  1897  1955  2152  2275  2328  2543
2735  2960
         15
1072  1234  1359  1613  1740  1868  1974  2122  2251  2360  2502  2631
2751  2876  3006
         15
1098  1200  1332  1478  1586  1719  1839  2011  2090  2215  2392  2475
2598  2795  3033
         14
1102  1195  1326  1485  1578  1709  1829  2020  2078  2203  2406  2459
2582  3054
          7
1258  1375  1454  1628  1748  1883  1952
          7
1127  1178  1485  1586  1726  1854  1984
          7
1028  1268  1381  1453  1613  1726  2011
          7
1027  1279  1381  1459  1613  1723  2014
          7
1031  1256  1381  1618  1742  1853  2011
          7
1029  1279  1394  1425  1642  1771  1974
          7
1052  1268  1377  1456  1748  1884  1950
```

Figure 4.8: Entry in the dst for the event shown in Fig. 4.5.

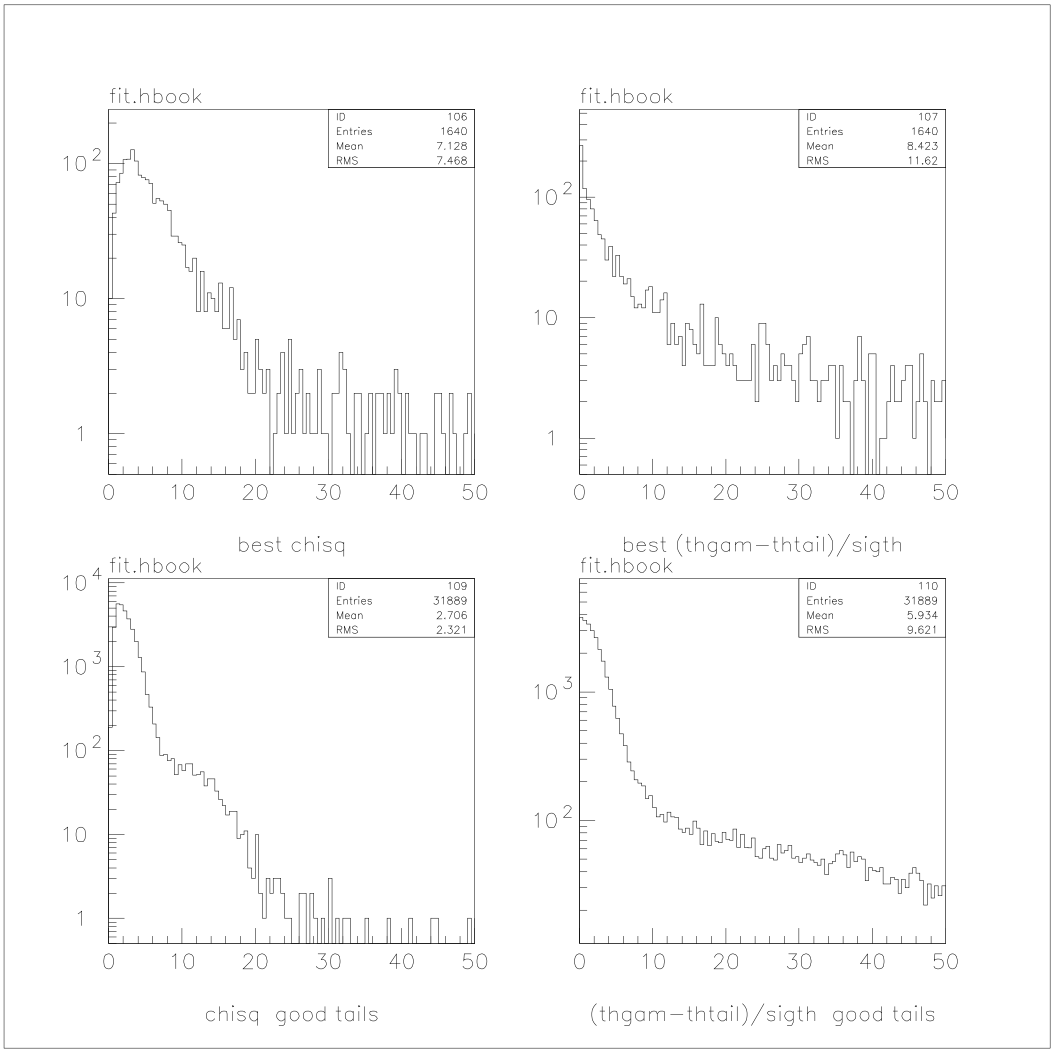

Figure 4.9: Histograms of χ^2 for the fit in v and of $\left|\theta_0 - \theta\right| / \sigma_\theta$ for re-fitted tails and good tails. Cuts were made of $\chi^2 < 7$ and $\left|\theta_0 - \theta\right| / \sigma_\theta < 8$.

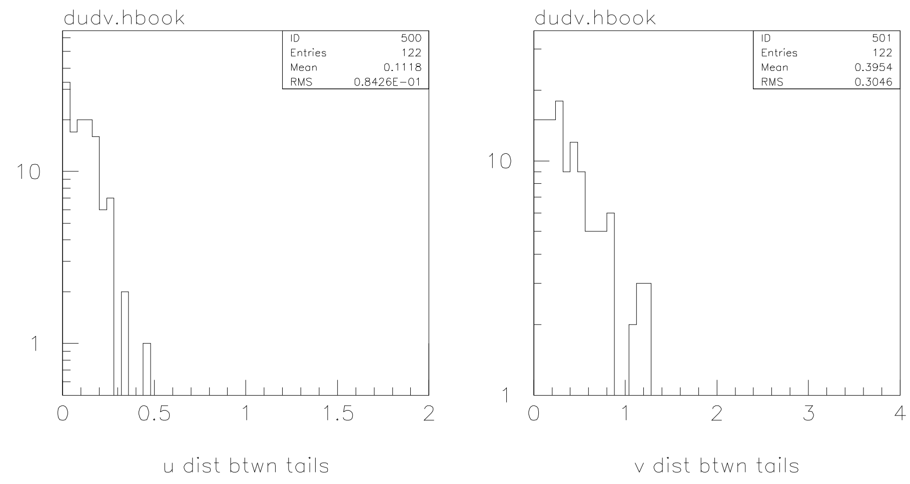

Figure 4.10: Distance in u and v between photon conversion tracks at the lead when there are two conversion tracks in GEANT.

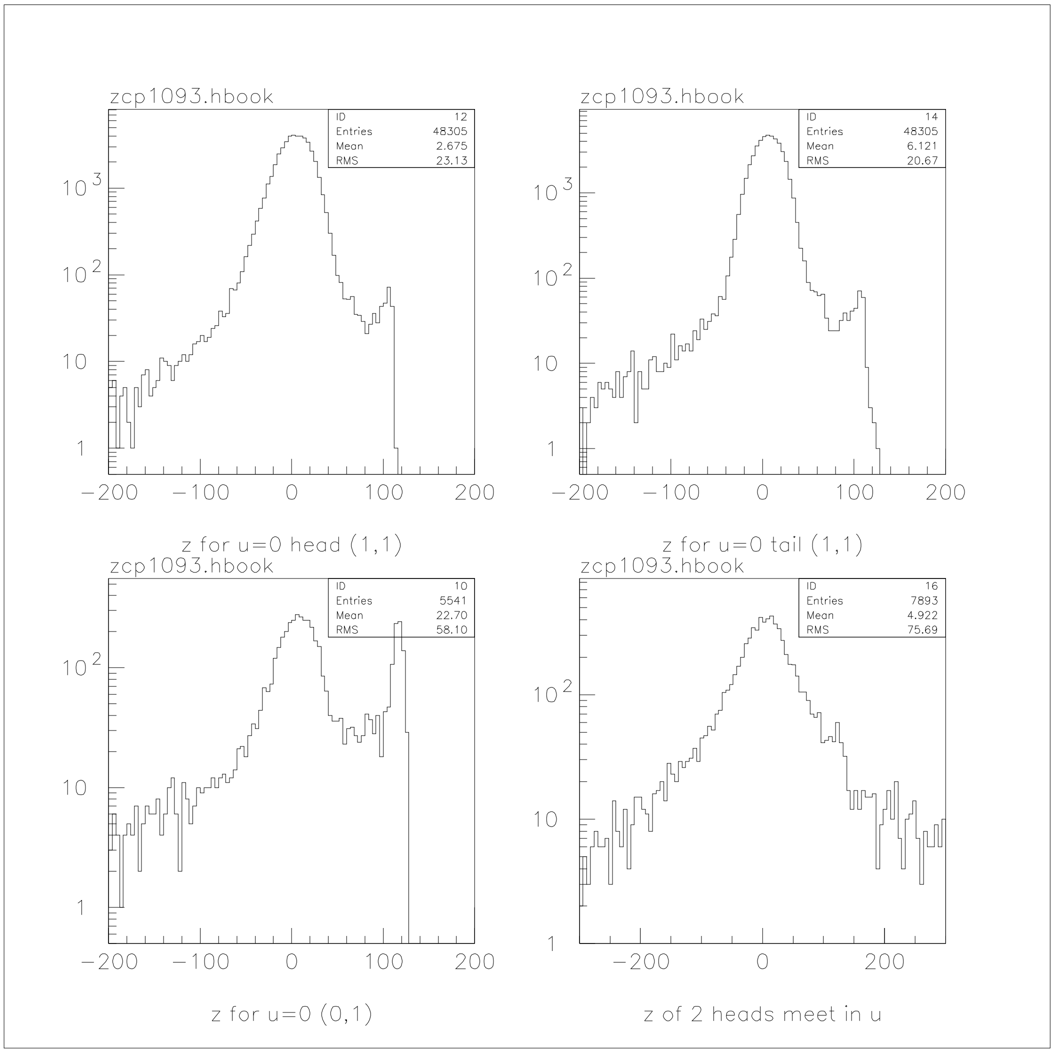

Figure 4.11: Pointing, defined as the z where the track goes through $u = 0$, for heads and tails of charged tracks, single photon conversion tracks, and the z where any two heads have the same u position, for lead-out run 1093.

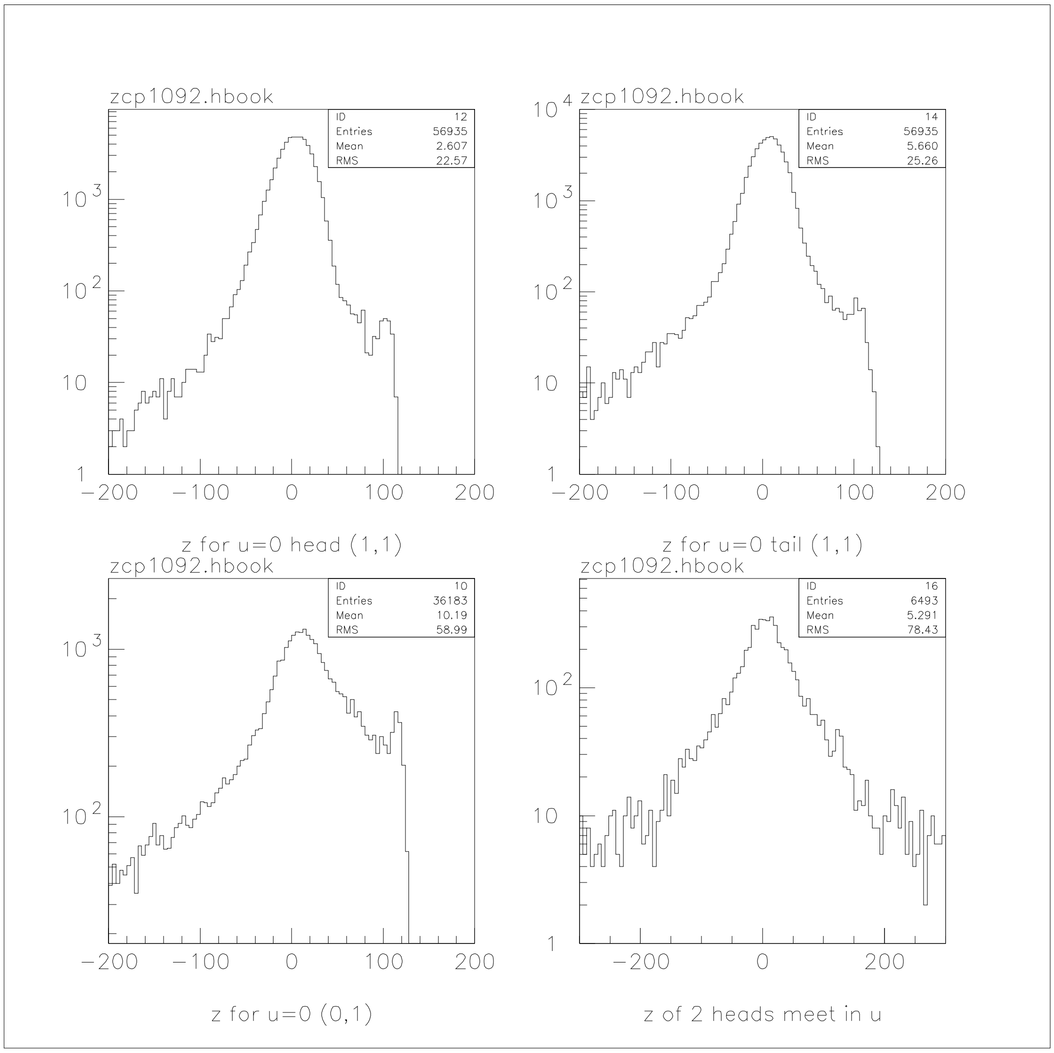

Figure 4.12: Pointing, defined as the z where the track goes through $u = 0$, for heads and tails of charged tracks, single photon conversion tracks, and the z where any two heads have the same u position, for lead-in run 1092.

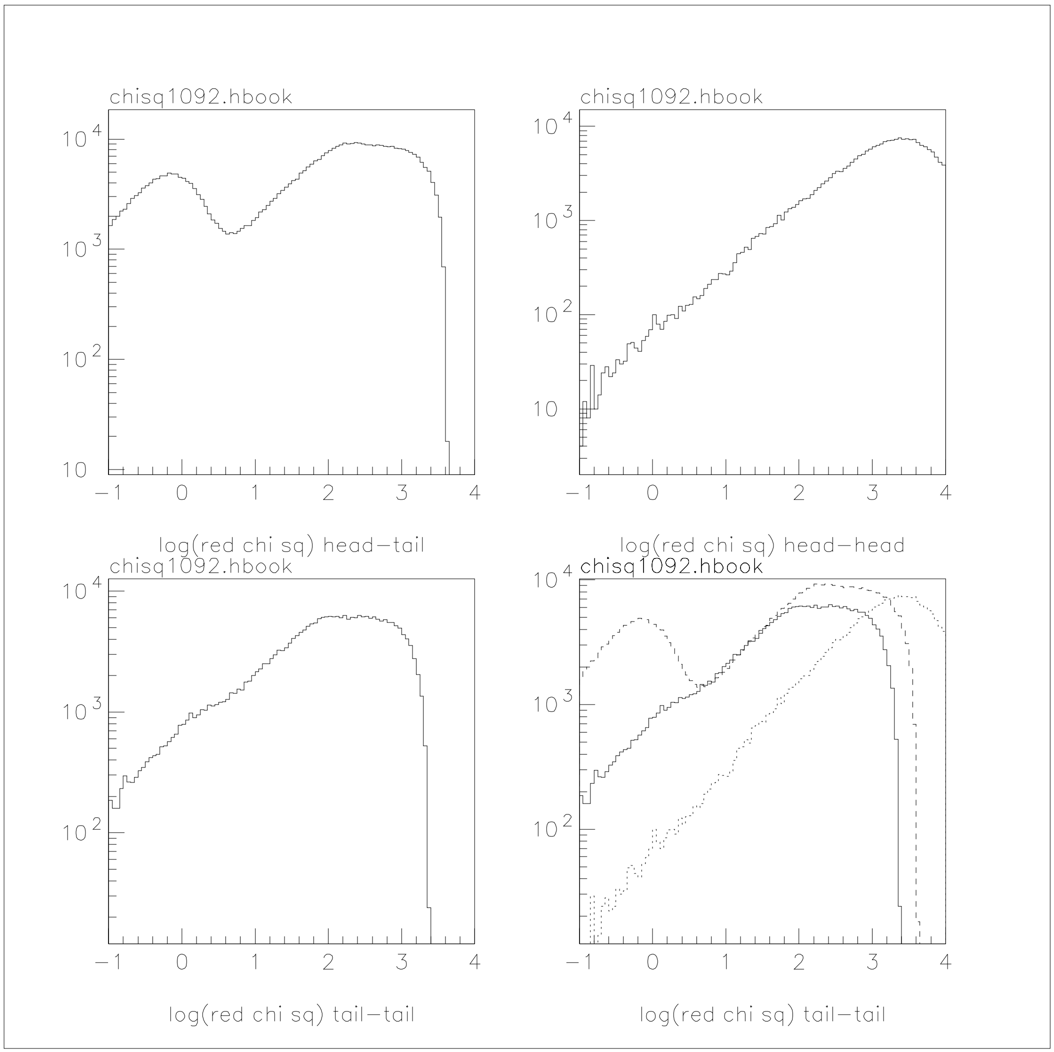

Figure 4.13: Values of $\log \frac{\chi^2}{2}$ for head-tail, head-head, and tail-tail matches at the lead. A superposition of these plots shows that $\log \frac{\chi^2}{2} = 0.7$, or $\frac{\chi^2}{2} = 5$ is a reasonable cutoff between matching real tracks together and track segments which are coincidentally close at the lead.

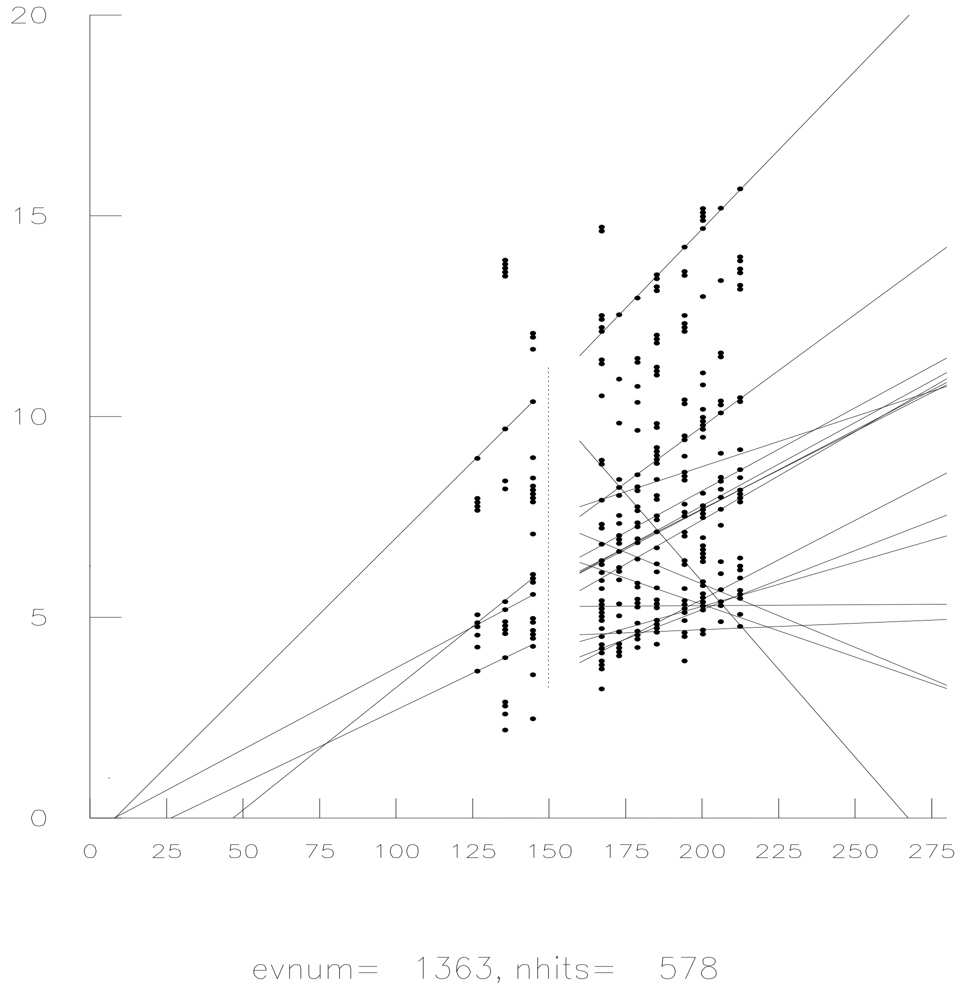

Figure 4.14: Display of the event shown in Fig. 4.6 for tracks kept by the vertexer.

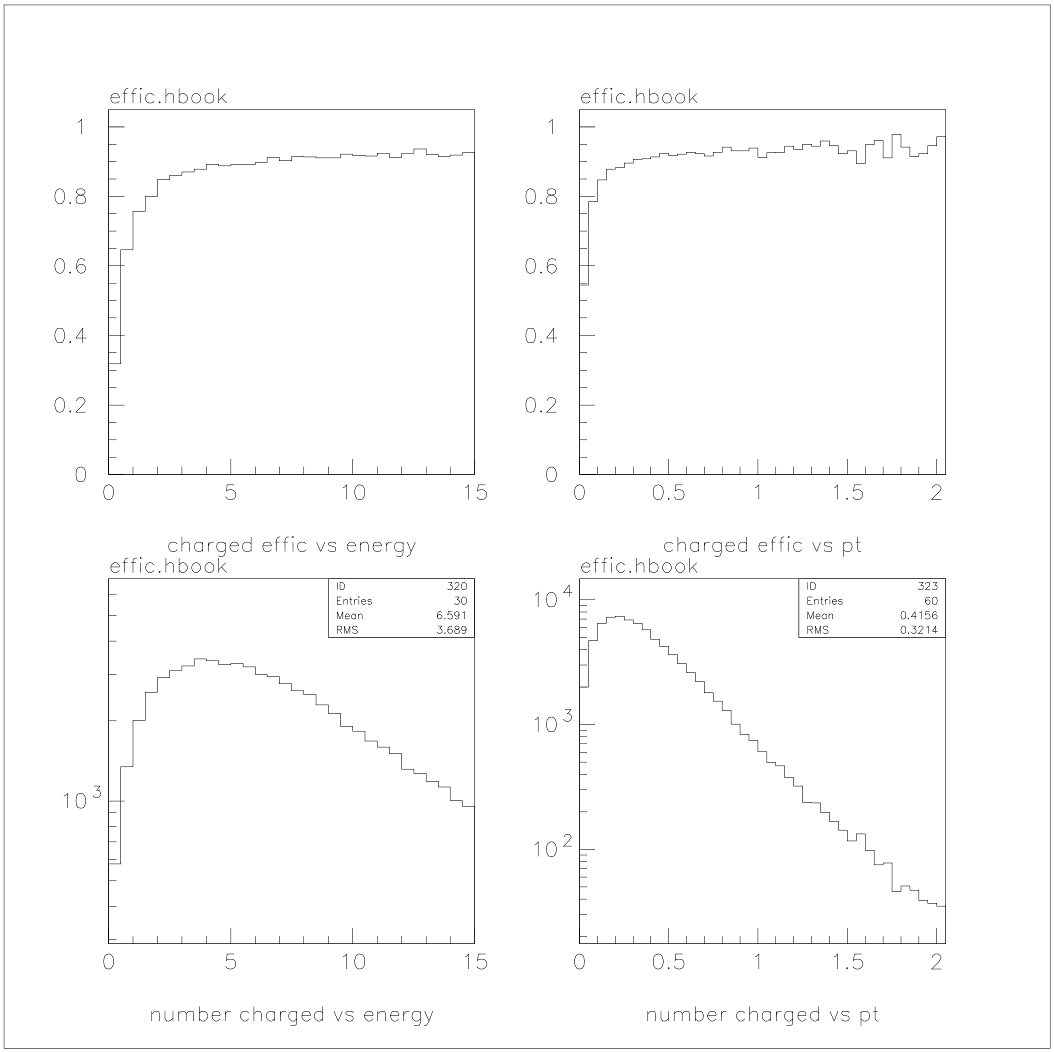

Figure 4.15: Efficiencies for finding charged tracks as a function of energy and transverse momentum of the track, number of charged tracks vs energy, transverse momentum.

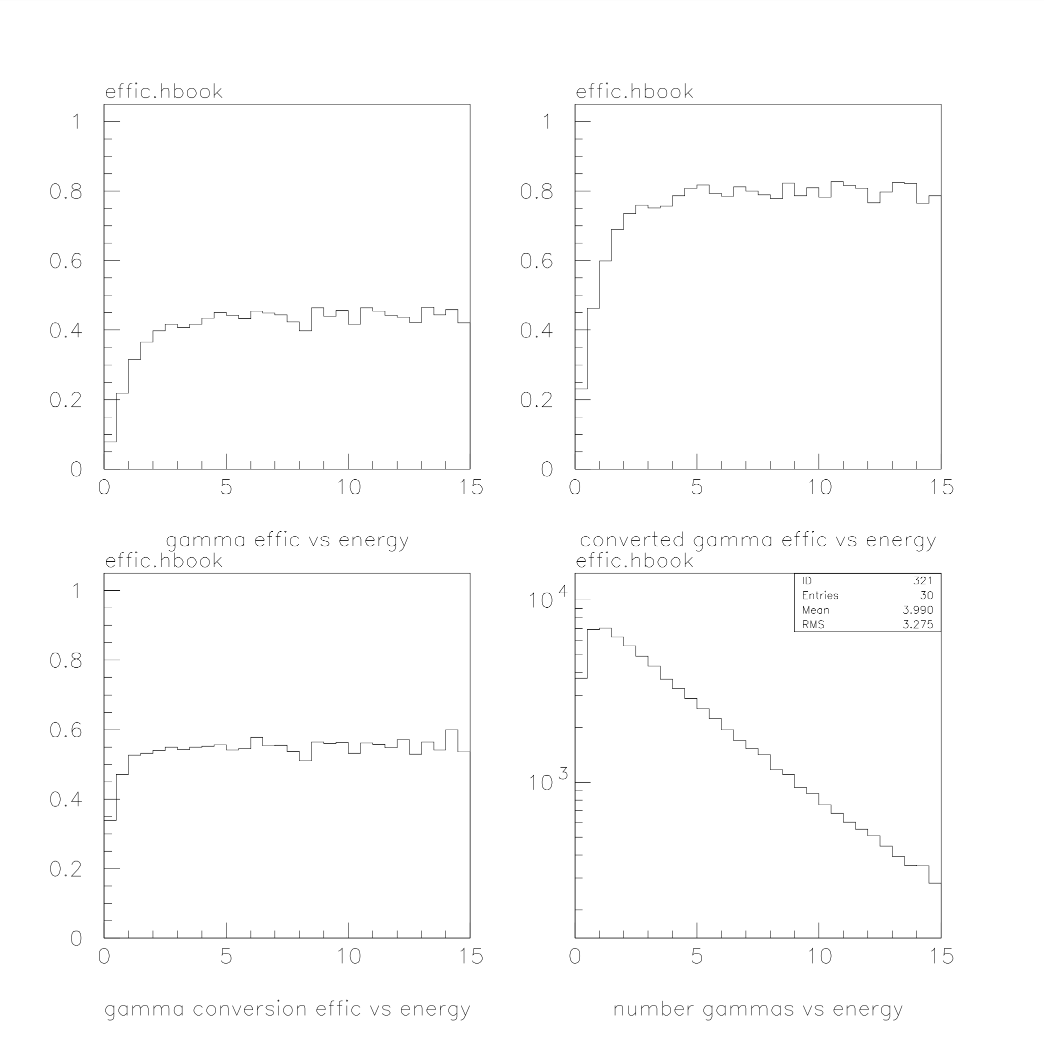

Figure 4.16: Efficiency for finding photons as a function of photon energy, efficiency for finding photons know to convert vs energy, probability of conversion of a photon vs energy, number of photons vs energy.

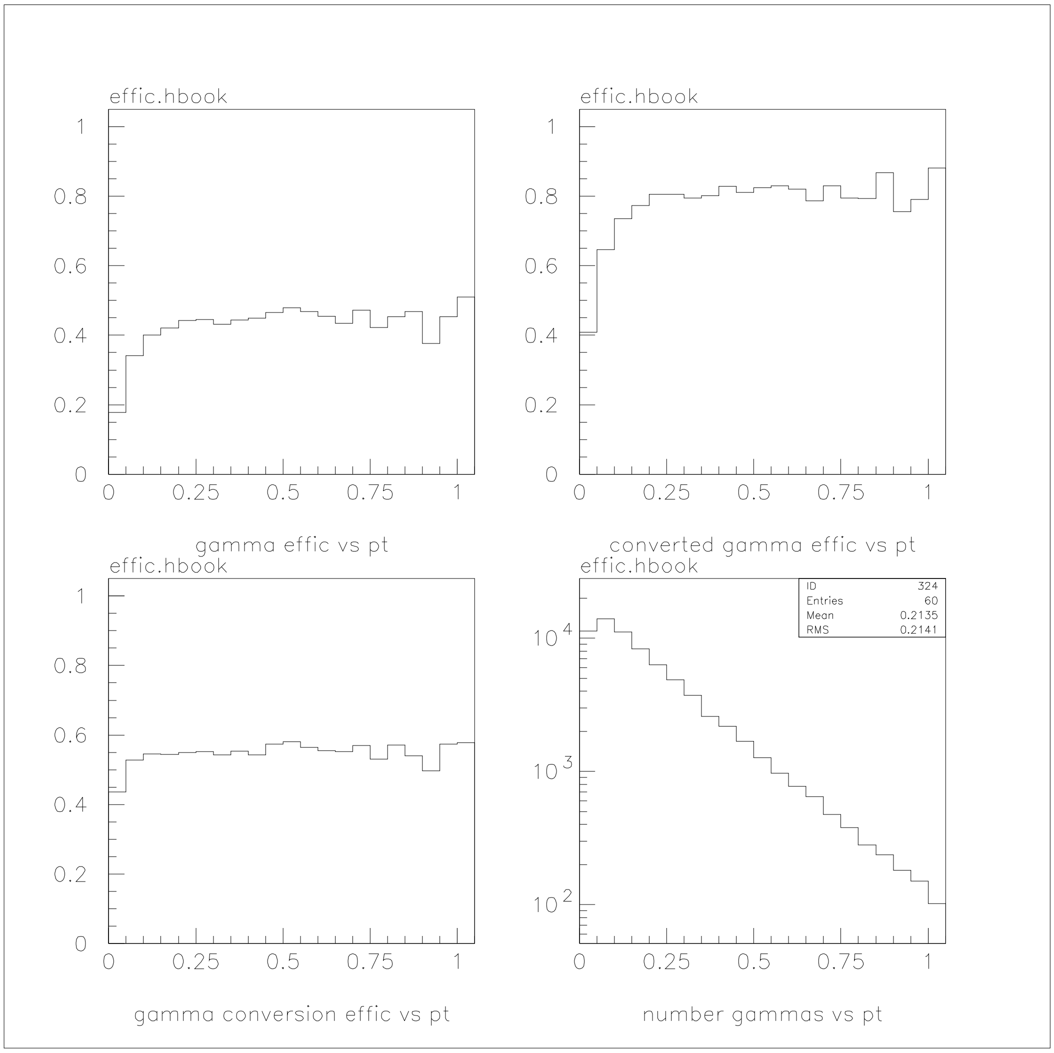

Figure 4.17: Efficiency for finding photons as a function of photon transverse momentum, efficiency for finding photons know to convert vs p_T, probability of conversion of a photon vs p_T, number of photons vs p_T.

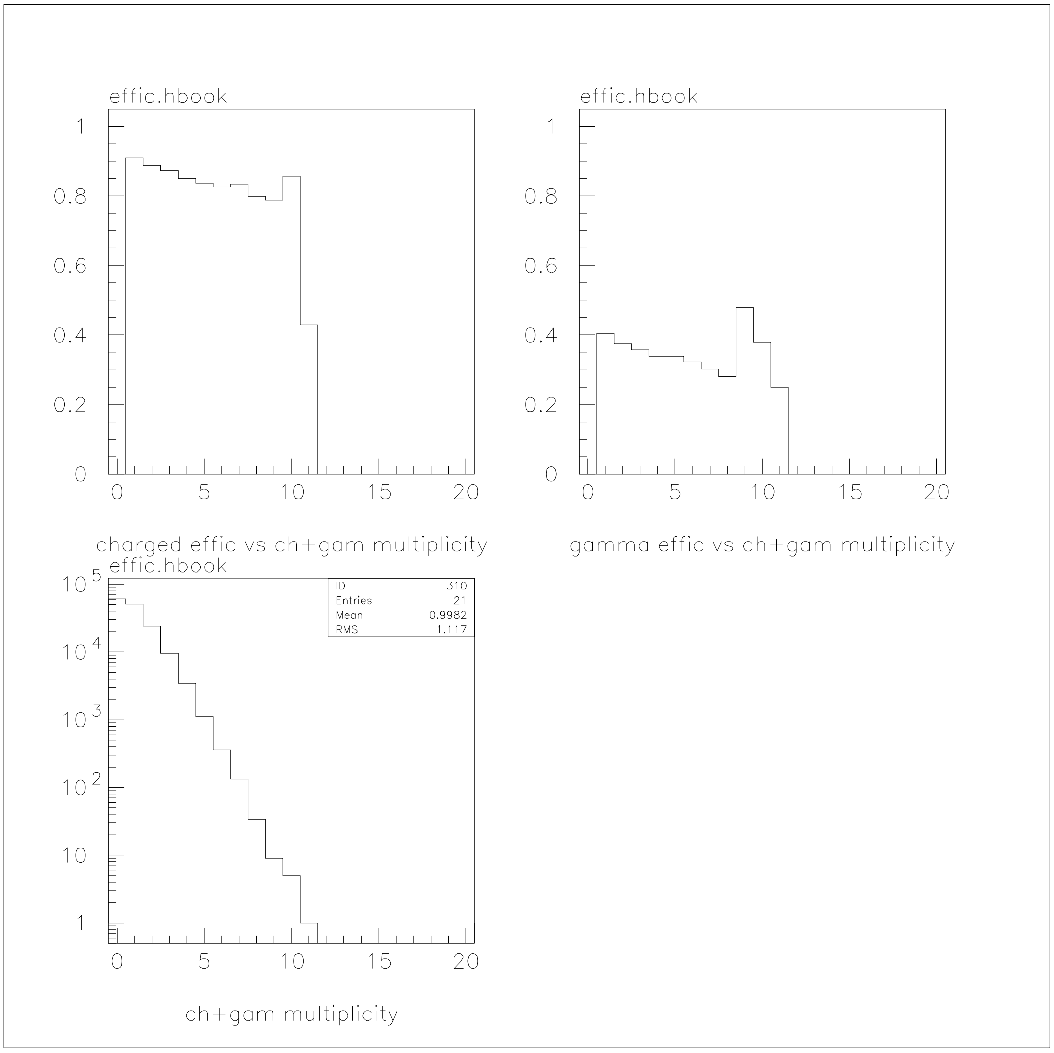

Figure 4.18: Efficiency for finding charged tracks as a function of total multiplicity into the acceptance, efficiency for finding photons vs total multiplicity, frequency of observing an event with a given total multiplicity.

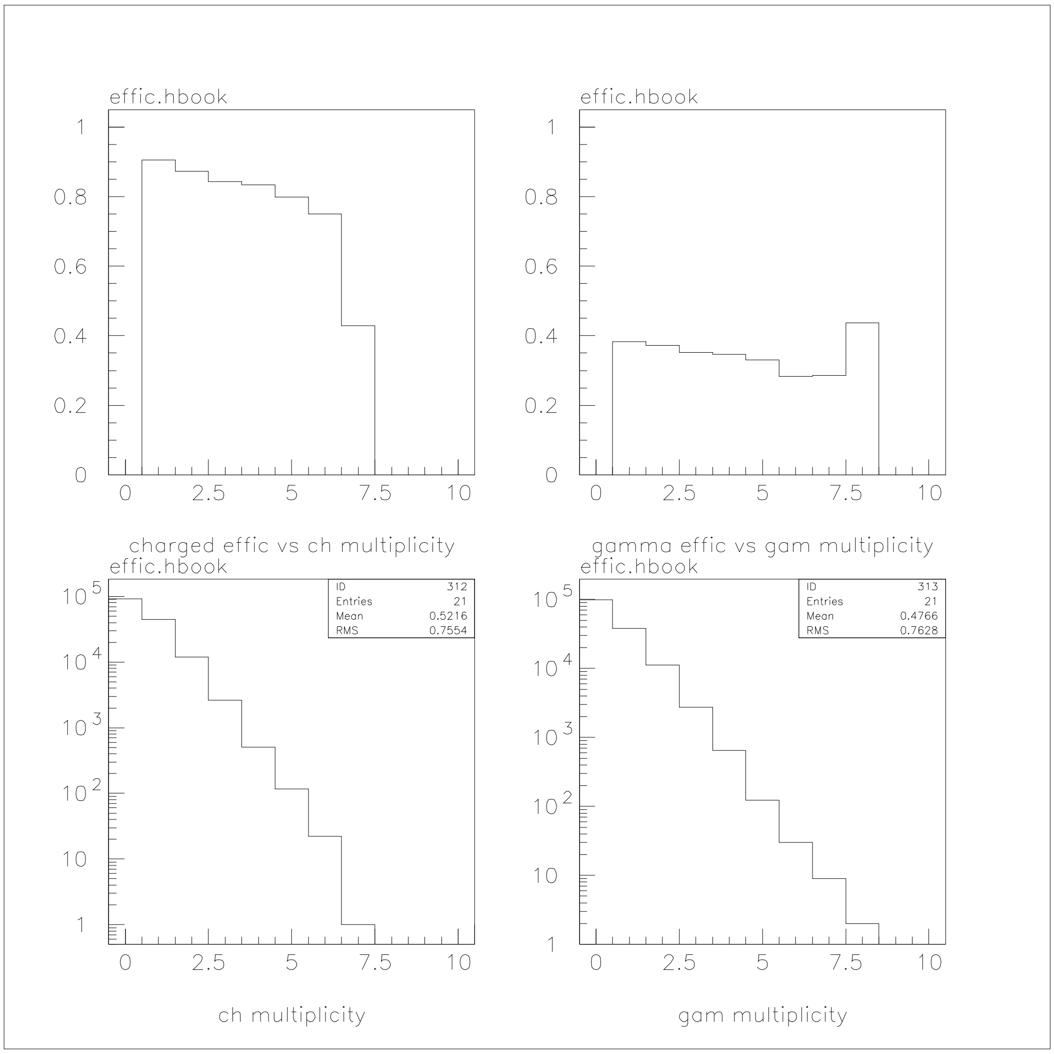

Figure 4.19: Efficiency for finding charged tracks as a function of charged multiplicity into the acceptance, efficiency for finding photons vs photon multiplicity, frequency of observing an event with a given charged multiplicity, frequency vs photon multiplicity.

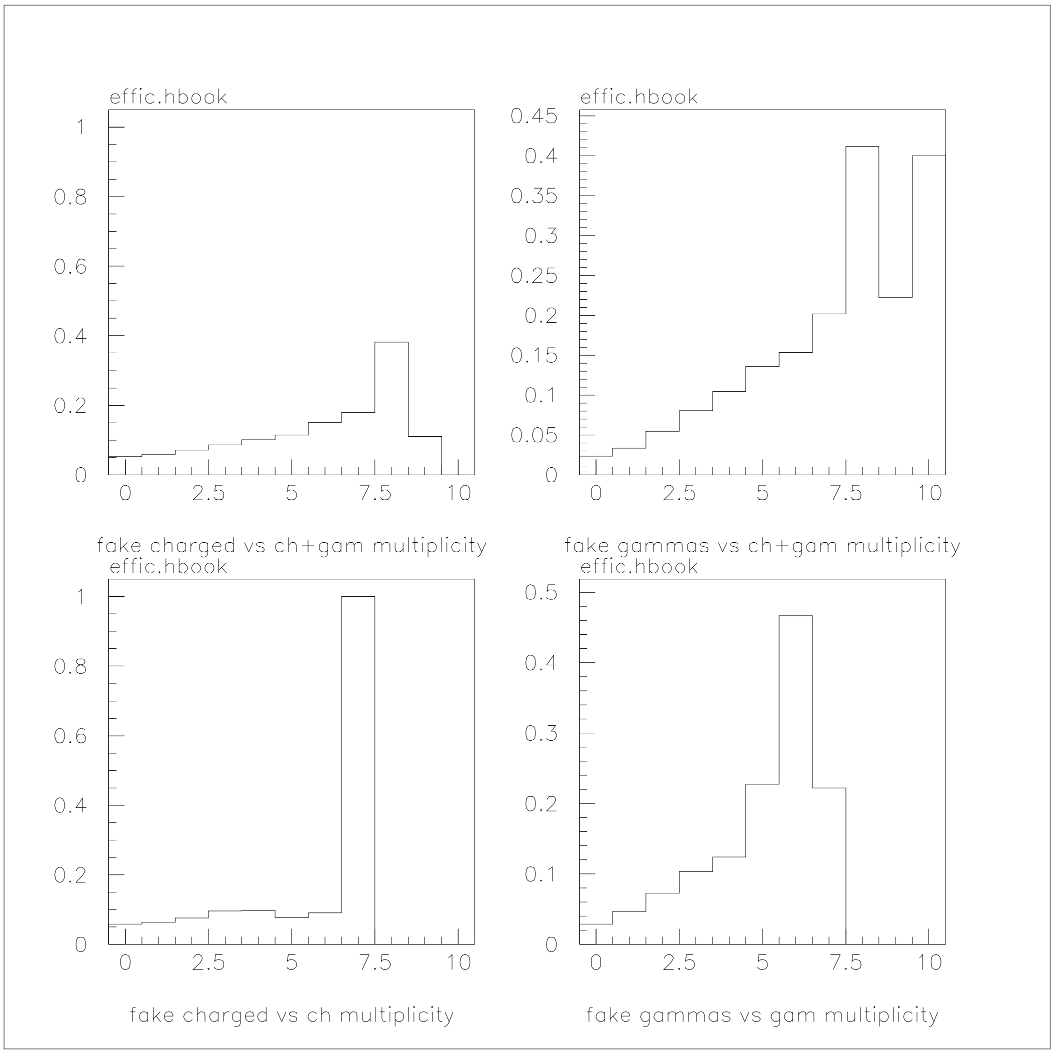

Figure 4.20: Mean number of fake charged tracks found per event with a given total multiplicity, mean number of fake photons found per event with a given photon multiplicity, mean number of fake charged tracks vs charged multiplicity, mean number of fake photons vs photon multiplicity.

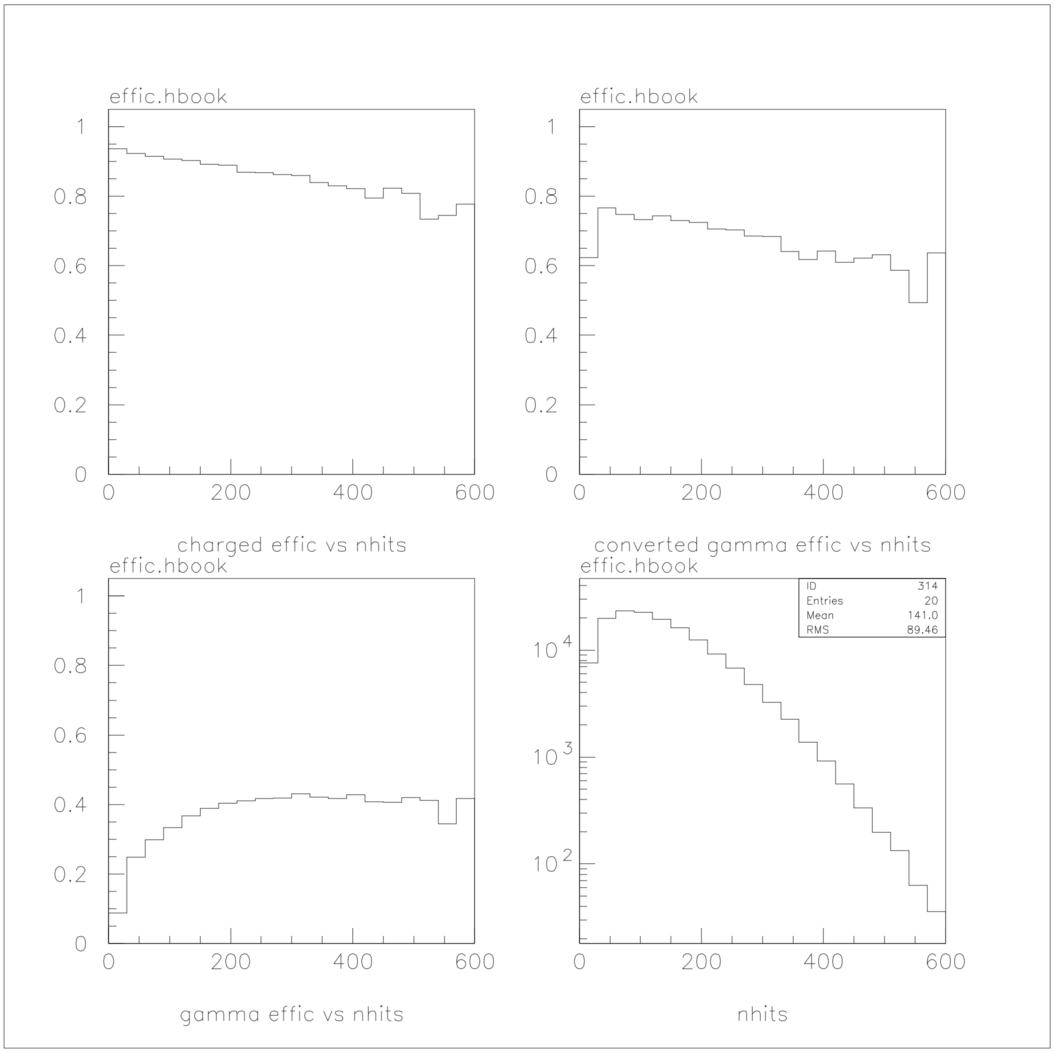

Figure 4.21: Efficiency for finding charged tracks as a function of NHITS of the event, efficiencies for finding converted photons and all photons vs NHITS, frequency of observing an event with a given NHITS.

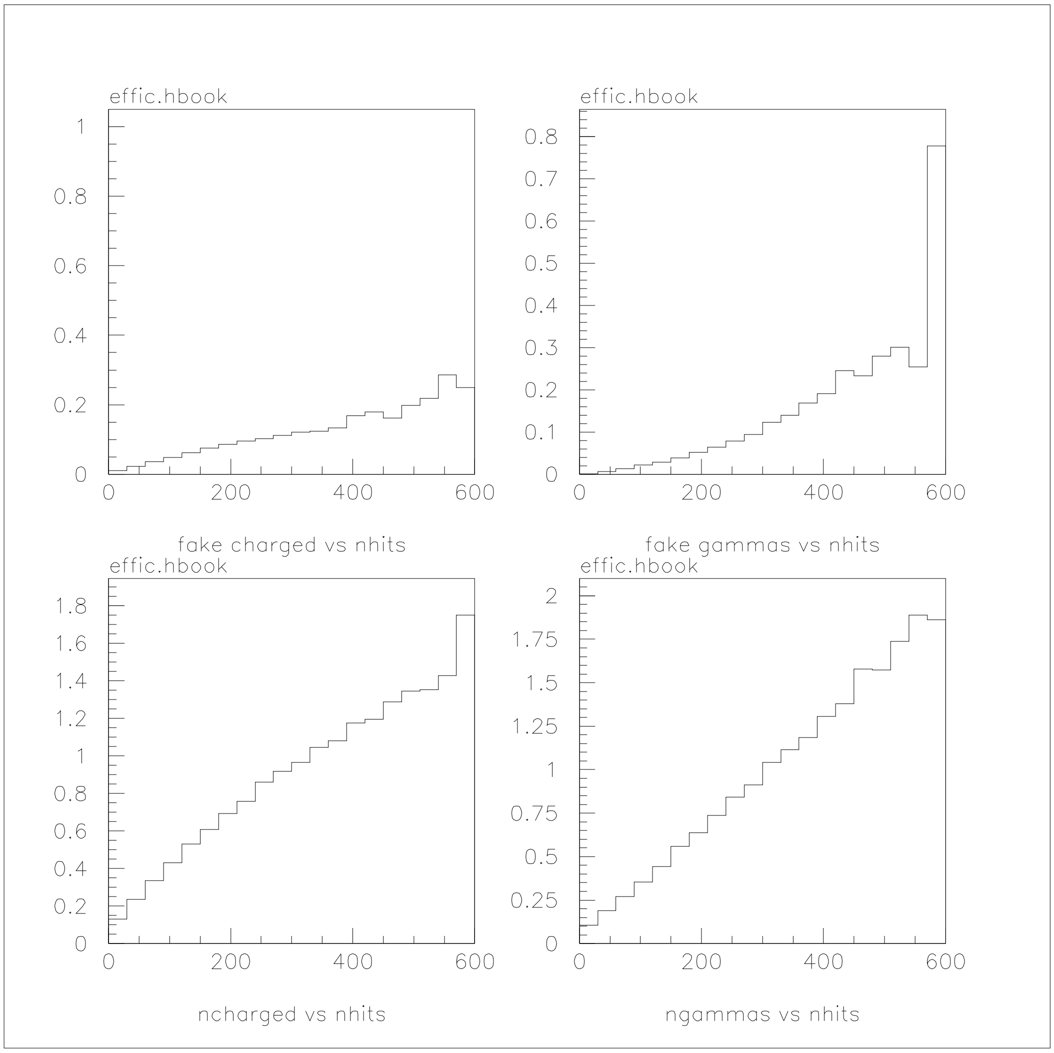

Figure 4.22: Mean number of fake charged tracks found per event with a given NHITS, mean number of fake photons found per event with a given NHITS, mean numbers of real charged tracks, real photons given NHITS.

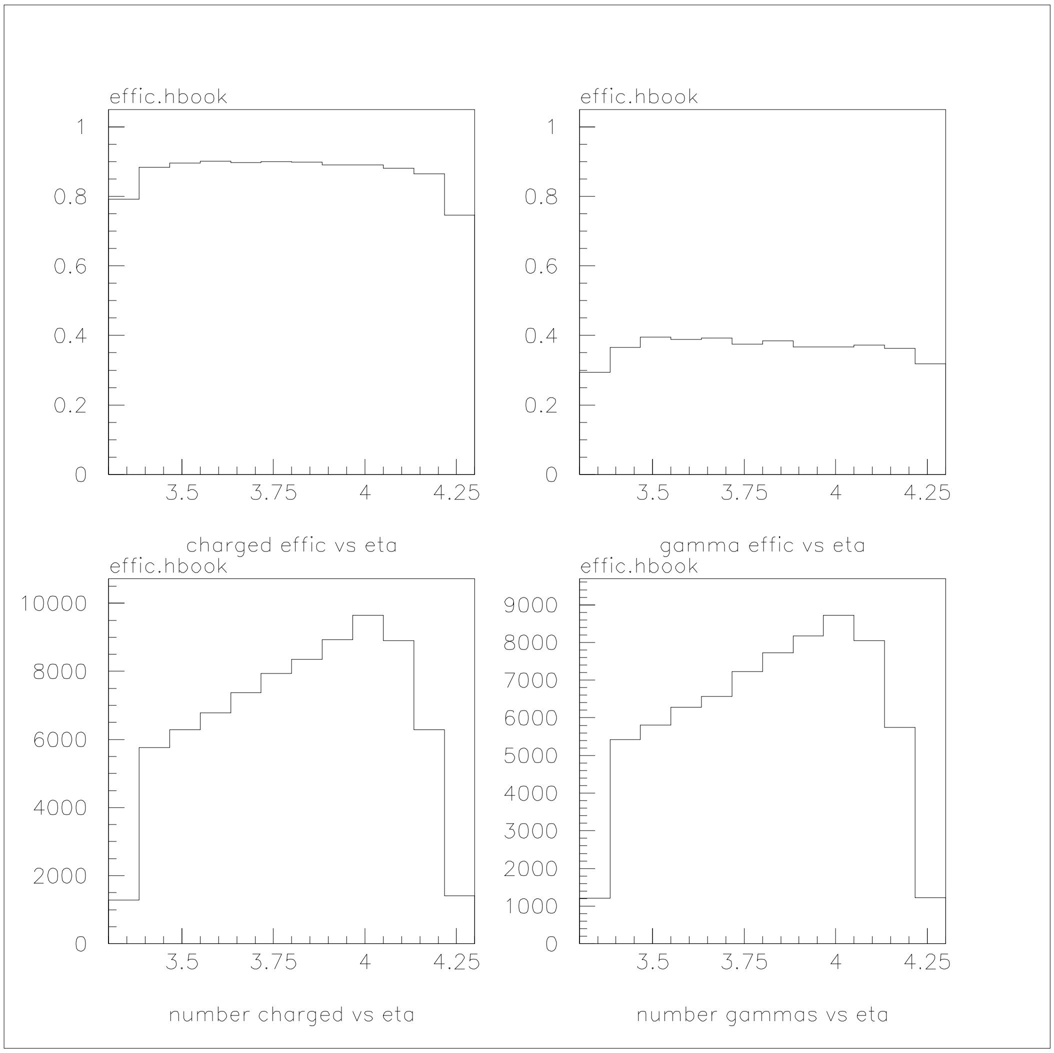

Figure 4.23: Efficiencies for finding charged tracks, photons at a given η, number of charged tracks, photons vs η.

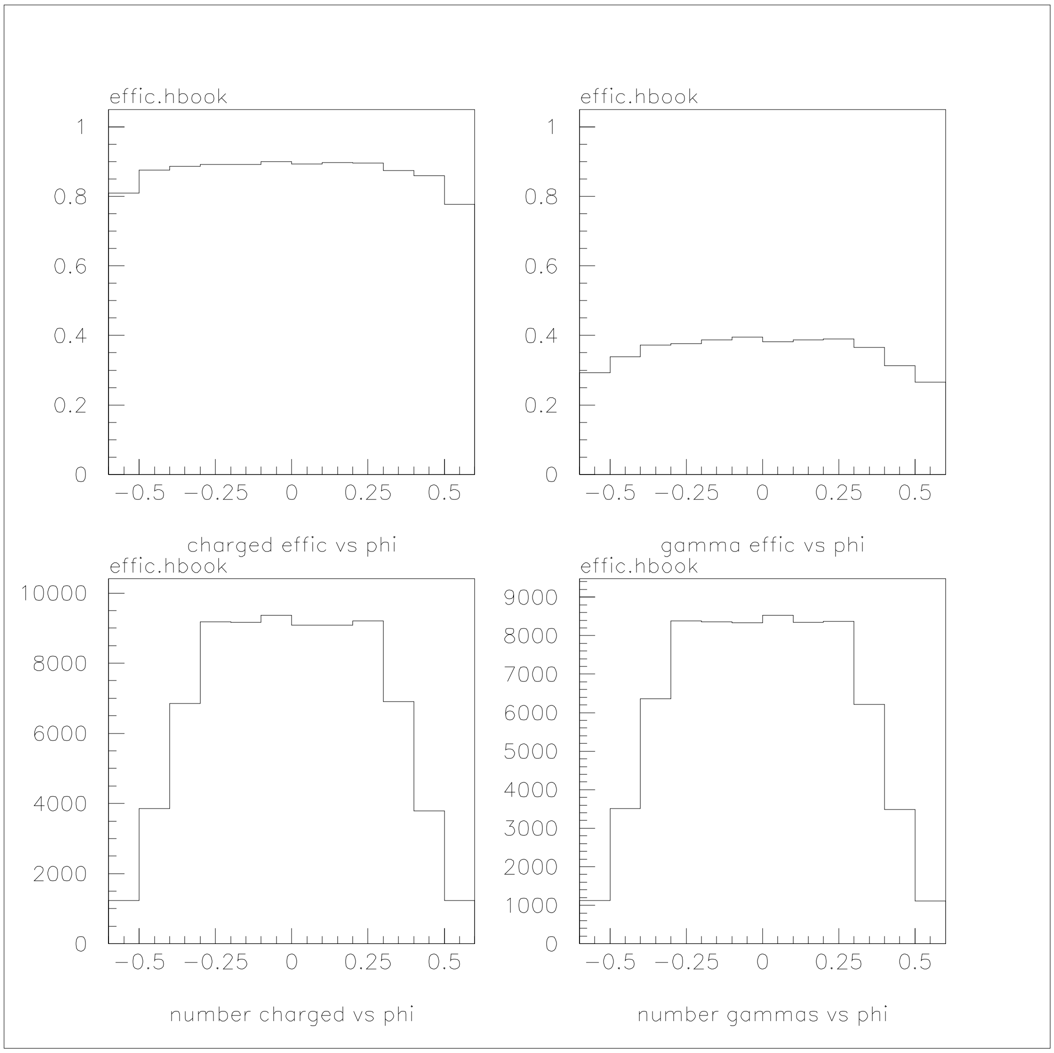

Figure 4.24: Efficiencies for finding charged tracks, photons at a given ϕ, number of charged tracks, photons vs ϕ.

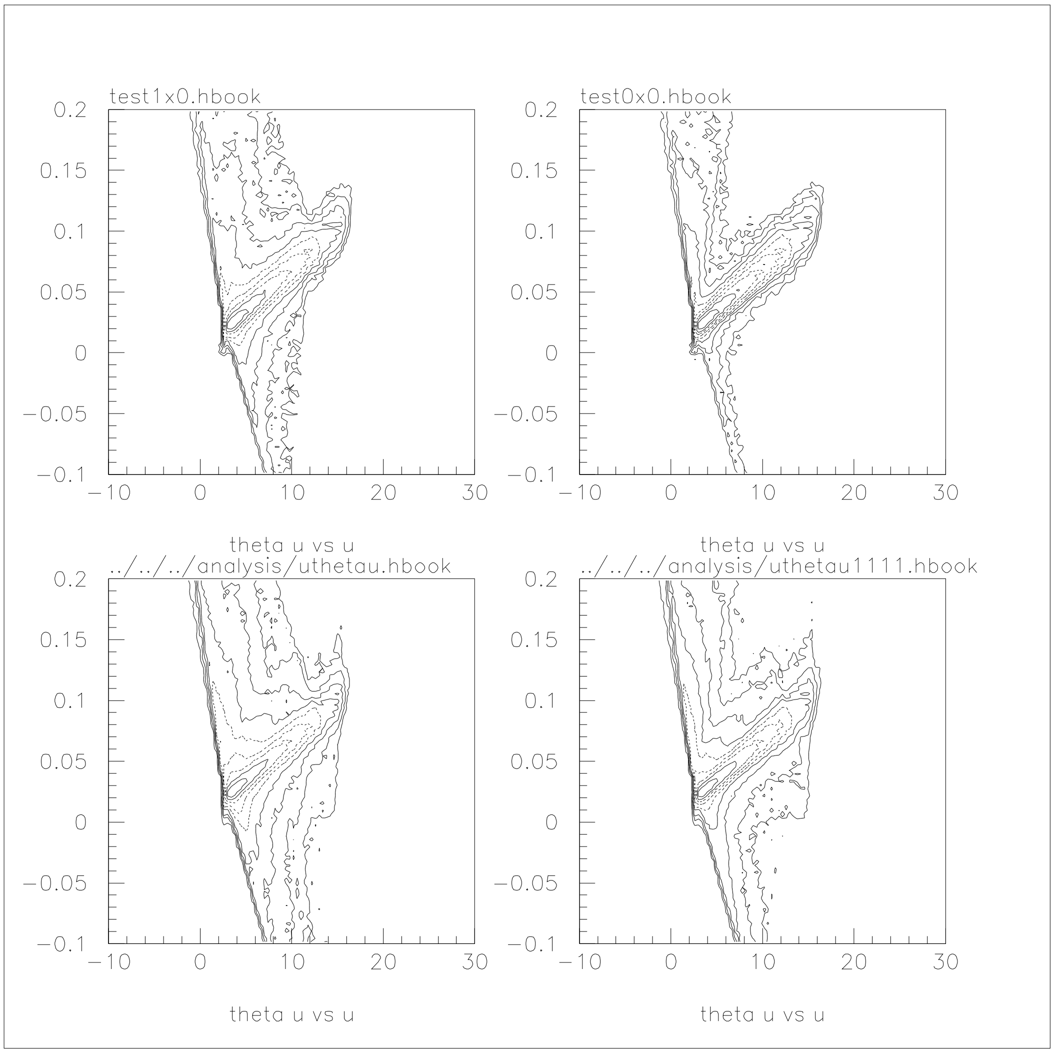

Figure 4.25: Location of tracks at the lead in phase space (u, θ_u) for lead-in GEANT, lead-out GEANT, lead-in run 1110, lead-out run 1111.

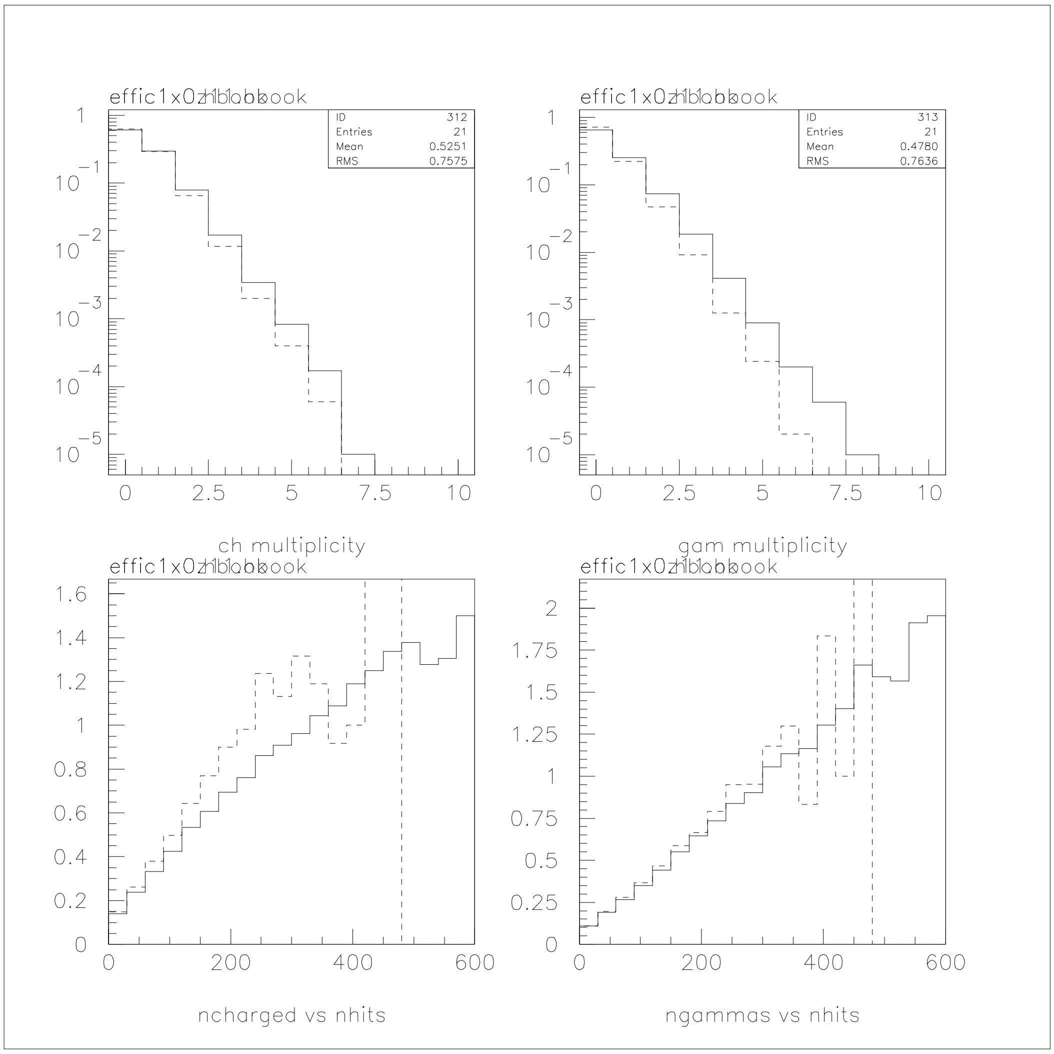

Figure 4.26: PYTHIA charged-track and photon multiplicity distributions, mean multiplicities vs NHITS for all lead-in GEANT events (solid) and for non-vetoed events (dashed).

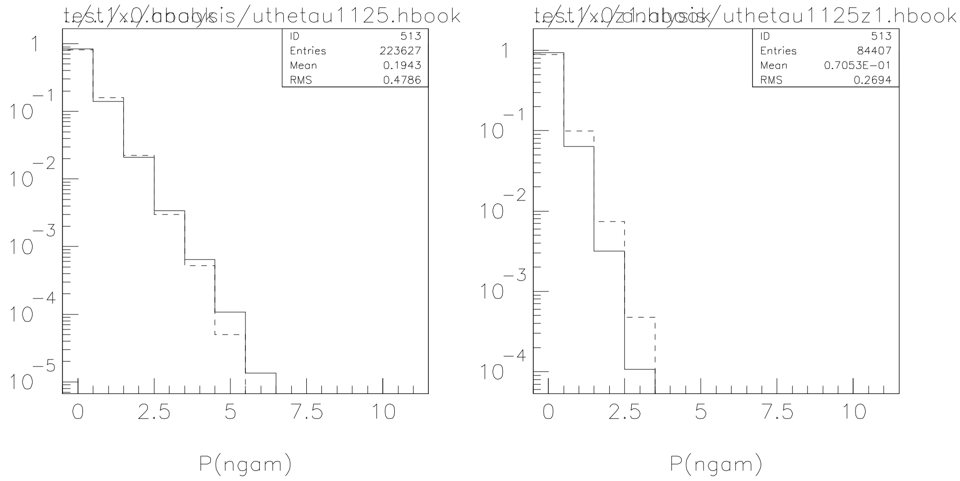

Figure 4.27: Observed photon multiplicity distribution for all events and for non-vetoed events from lead-in run 1125 (solid) and lead-in GEANT (dashed).

track type	chambers searched	number of chambers hit	used-wire cut	grouping cut
charged	1-24	≥ 22	17	16
		21	17	16
photon/ ch tail	9-24	≥ 15	13	11
		14	13	11
mid-8	9-16	≥ 7	5	6
front-8	1-8	≥ 7	5	6

Table 4.1: Cuts used by the tracker.